



Digital to physical development of a reconfigurable modular formwork for concrete casting and assembling of a shell structure

Odysseas Kontovourkis*, Marios C. Phocas, Constantinos Katsambas

Department of Architecture, Faculty of Engineering, University of Cyprus, 75 Kallipoleos Str., P.O. Box 20537, 1678 Nicosia, Cyprus

ARTICLE INFO

Keywords

Computational design optimization
Fabrication
Sustainable workflow
Free-form shell structure
Reconfigurable formwork

ABSTRACT

This paper demonstrates an integrated computational design and fabrication workflow, implemented in actual construction scale, in order to test its feasibility towards a productive and customizable manufacturing process. The project suggests the computational development and the semi-automated fabrication of a free-form shell structure that consists of customized concrete members. The development process is based on two pillars of investigation that are bi-directionally connected; the computational design optimization and the fabrication. The first part of investigation refers to the form-finding of the overall shell structure, as well as its structural members by using topology optimization principles. The second part deals with the development of a reconfigurable modular formwork, which adapts to all shape alternations of the structural components, enabling their effective fabrication by using a single mechanism. Within this framework, decisions taken in the optimization stage are evaluated based on limitations and potentials of the suggested formwork, whose reconfigurability influences fabrication outcomes and vice versa.

Introduction

Nowadays, computational design and fabrication processes, apart from their experimental implementation in architecture, design and relevant arts, are progressively applied in real scale design and construction [1–3]. The viability of innovative tools and processes plays a decisive role, both during the design, as well as their actual construction stage, due to the need for developing and producing results that meet a number of limitations or criteria related to structural stability and constructability [4]. This shift towards real-world applications cannot be implemented without careful and detailed consideration of the sustainable aspects of solutions, in terms of their ecological and economic impact [5,6]. Within this framework, the concept of mass-customization plays a fundamental role since it directs the production process towards adaptive forms and systems according to specific needs and demands [7]. Nevertheless, such focus is necessary to be included within a new framework, where viability of processes and results obtained are carefully considered. Currently, an important direction in this area of research is the control of design intentions through optimization principles, aiming at material waste minimization [8,9]. This allows reduction of materials and therefore, minimization of their cost, leading to the economic feasibility of solutions, and as a consequence, improving the environmental impact of structures. All the above are inseparably linked with the feasibility of construction methods applied. In case of

automated approaches, their application can reduce material waste and minimize energy consumption during the construction process, achieving in parallel construction accuracy [10].

Computationally controlled optimization processes trace back to examples where the design of efficient structures has been influenced and inspired by natural principles [11–19]. In this frame, topology optimization, has been progressively implemented in the last years, for the development of optimum structures with maximum stiffness and minimum material consumption [20,21] with popular algorithms to be among others the Solid Isotropic Microstructure with Penalization (SIMP) and the Evolutionary Structure Optimisation (ESO) [22–25]. Recent developments in advanced fabrication, and particularly in the growing field of Additive Manufacturing (AM), open possibilities for integrated topological optimization and fabrication processes, which can be implemented in various fields including architecture and engineering, either in small, medium or large-scale construction [8]. A closer relation between topology optimization and AM can be established to resolve design constraints during production [23] and overcome current obstacles in the area of manufacturing [26]. Examples like the ‘Light rider’ and the ‘AM node’, prove that a great amount of material can be saved from parts of a structure compared with the conventional fabrication approaches. In the case of ‘Light rider’, the frame of a motorbike was optimized and 3D printed using aluminium alloy, while in the case of ‘AM node’ a complex cable connector node was optimized and 3D

* Corresponding author.

Email address: kontovourkis.odysseas@ucy.ac.cy (O. Kontovourkis)

printed with steel. In both cases, the final organic shape of material optimized structures showed that stiffer and stronger structures can be obtained, if this is correlated with the conventional ones [23,26,27].

In large scale and particularly, in construction of entire buildings and structures, limited number of examples can be found where topology optimization and manufacturing processes are applied. The majority of such examples appears in linear manner and in the initial stage of the design decision-making process followed by the production of building parts using conventional manufacturing approaches. In Akutagawa River Side project, the ESO optimized approach has been used during the design of two side walls, followed by their construction with reinforced concrete material using large custom-made formworks [28]. In the case of Qatar National Convention Centre (QNCC) in Doha, a tree-like structure that supports 250-m-long and 110m wide lobby roof was designed by implementing the Extended ESO algorithm [29]. The basic tree-like structure was built by producing a complex structural system consisting of a simplified structural core of octagonal tubes of flat steel profiles, and a number of single and double curvature steel panels for the exterior skin [30].

Currently, several attempts to introduced topology optimization principles in the design development of actual non-standard forms have been conducted. Also, a number of parametric design plug-ins have been introduced, such as Millipede [31,32] and Ameba [33], both plug-ins for Grasshopper [34], a parametric design add-on for Rhinoceros 3D [35], attempting to achieve a more direct relation between design and fabrication. Projects like 'Unikabeton' and 'OptiCut' [36,37] have been developed based on design investigation using topology optimization principles and subsequent fabrication of self-compacting concrete structures using polystyrene formworks, which have been produced through CNC milling and hot wire cutting [37].

Although, current attempts to integrate design optimization and automated fabrication have grown in number, examples show that the existing methods applied, particularly in fabrication stage, are one-off construction solutions leading to expensive and complicated custom-made components or formworks. In addition, the majority of the current built projects that uses topology optimization for form generation, have used complicated and costly formworks for their construction, which does not seem to follow the main objective of material minimization. In order to overcome this and to eliminate material waste and cost during the process, as well as to find an effective method for manufacturing highly differentiated modular shapes and their mass-customized logic, current attempts to introduce adjustable, adaptive or reconfigurable formworks in the fabrication process are coming to the fore [38–41]. Such examples can be found, for instance in the work 'Slipforming', which demonstrates an automated and robotically-driven mould mechanism that can be adjusted according to predefined complex designs of free-form columns [3]. Also, in 'Procrystalline Wall' project, where more than 400 differentiated concrete cells have been designed and fabricated using a single digital mould [42] and in 'Mars Pavilion', where two industrial robotic arms are used for manipulating fabric sleeves, creating an adjustable formwork into which concrete is poured for rapidly producing object variations [43]. Finally, in the project 'Robotic Casting' a variable family of structural modules is achieved by rotating the mould and by using a 6-axis robot [44].

The analysis of cost and construction time through automation is an important element in developing such mechanisms in order to assess

their feasibility. Towards this direction, studies have been carried out to compare conventional and automated methods, which among others include the work by [45] on economic evaluation of robotic applications in building construction, the work by [46] on the development of an expert system to support decision-making in regard to the application of robotics in construction or the work by [47] that demonstrates and compares the cost and time of fabricating a robot built wall. With regard to the formwork construction, the cost of conventional approaches is approximately estimated at 10% for the total cost of the building and at 40–60% for structural systems [48]. In particular, the cost of formworks for shells is estimated at 30–40% of their overall construction [49], which, in the case of free-form shells, is dramatically increased, especially in regard to labor cost [50]. A series of cost estimations regarding construction of free-form shells, and in particular the development of formworks for concrete casting can be found [38,51,52], however the development of comprehensive methods to analyse the cost or time of formworks construction in order to increase productivity are very limited and is influenced by local or regional factors including cost of materials, labor cost, and so on. All the above have prevented the expansion and development of this type of structures [38], despite the fact that automation and robotics have been introduced into the construction to overcome such obstacles, for instance by the use of flexible formworks [49,53]. This is more obvious nowadays, where a growth trend in the design and fabrication of free-form structures is observed based on such manufacturing mechanisms, which seems to have no corresponding response in the way are being implemented in order to reduce cost and construction time.

This paper aims to establish an integrated computational design approach based on topology optimization principles for material reduction of a shell structure and a subsequent fabrication process through the development of a reconfigurable modular formwork for concrete casting of modular units. It also aims to examine customization and productivity of the proposed approach and asses its cost and construction time. Firstly, a general description of the methodology introduced in this paper is given. Then, three distinct investigations are conducted; first, the parametric design control and structural analysis experimentation leading to shape optimization, second, the adaptive fabrication process, which involves the production of a reconfigurable formwork mechanism in actual scale, and third, the manufacturing process and the physical prototyping results in actual scale. Through quantitatively results and critical review on the benefits that an automated fabrication approach can bring to the conventional construction industry, this study aspires to explore the prospect of deepening into the fabrication of complex structures in actual scale.

Methodological framework

The suggested integrated methodology is developed around the idea of a reconfigurable formwork system that is driven by computational design based on topology optimization principles. In particular, the methodology targets towards material minimization of a concrete shell structure at digital design and physical construction level of investigation. Analytically, the design optimization approach aims at achieving minimization of the material used and hence at contributing towards less environmental impact solutions. The development of the modular formwork system refers to the reconfigurable physical prototype. The suggested computational workflow consists of three interrelated parts of investigation (Fig. 1).

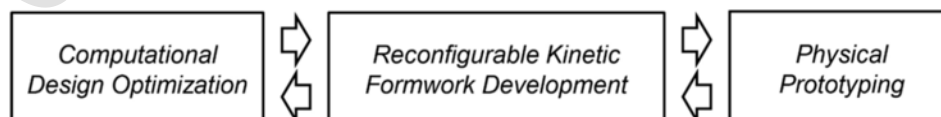


Fig. 1. Overall framework of research investigation.

In the computational design optimization stage, the geometrical configuration of shell structures based on a form-finding process and the design investigation based on topology optimization principles is conducted. Two experimental case studies (ECS) are demonstrated that involve all or some of the following computational design steps:

- Form-finding and design tessellation of the overall shell structure
- Design optimization approach that includes topology optimization principles and static analysis
- Detailed design development

In the first step, a form-finding process for the development of shell structures is conducted using the Kangaroo plug-in [54], a physics-based engine in Grasshopper plug-in [34] for Rhinoceros 3D [35]. In the second step, topology optimization principles are applied using the Millipede plug-in [31,32] for Grasshopper and the structural Finite-Element Analysis (FEA) software SAP2000 [55]. In this step, the process of material minimization based on the results of topology optimization is investigated. Finally, in the third step, the detailed design of the overall shell structure is developed using Rhinoceros 3D. Fig. 2 shows the computational design steps undertaken.

In the reconfigurable modular formwork development stage, the design of semi-automated formwork is developed. The construction process and the selection of the mechanical parts comprising the overall system are explained. This is accompanied by an analytical explanation on the geometrical typologies that the reconfigurable system can achieve through its reconfigurability according to the given design task. The whole range of geometrical configurations are modelled in the parametric design environment of Grasshopper plug-in.

In the physical prototyping stage, the operating procedure of the reconfigurable mechanism is analytically presented. The process of shape adjustment, concrete casting and demoulding are the three phases incorporated. This is repeated according to the number of structural modules that are to be constructed. In this phase of experimentation, discussion on the assembly of modular structural members under investigation is also included. Finally, a feasibility study to compare cost and construction time between conventional and suggested reconfigurable formwork mechanism in shell structures construction is developed.

Computational design optimization

In this chapter two experimental case studies (ECS) in terms of design optimization have been conducted. Aim was to seek for limitations and potentials of each experiment, in order to select the appropriate workflow that would provide digital design results that would be physically realized. In parallel, the selection of the appropriate workflow acknowledges the difficulties of the tasks involved during the construction phase, where a thorough and accurate fabrication process is necessary, and at the same time, the involvement of a low-tech/cost mechanism for rapid manufacturing execution is required. Within this frame, an examination over optimization and large-scale construction of free-form shell structures shows two basic directions of investigation. The first direction deals with the production of structural nodes. In the case of 'Smart nodes' project [56], topology optimization is followed by a

fabrication process and specifically Additive Manufacturing (AM) in order to produce canopy's structural nodes, which are used to link simple standardized beam elements and planar panels [56]. Also, in [57] a novel assembled hub joint with good mechanical performance and economic benefit is introduced in order to satisfy the demand for industrial assembly of single-layer reticulated domes. Furthermore, two design approaches have been proposed to design structural nodes of complex shapes for grid shell structures, seeking improved structural performance and design efficiency by using the transitional section method and the bi-directional evolutionary structural optimization method, respectively [58]. Similarly, other methods that involve topology optimization in conjunction with robotic construction procedures, try to simplify or standardize the structural elements, yet allow a custom logic to come to the fore towards the feasibility of the construction process.

In this paper, two experimental case studies (ECS) have been distinguished based on the structural components of the shell structure to which the topology method has been applied, as follows:

- Nodes' topology optimization and members' standardization (ECS A)
- Members' topology optimization and nodes' standardization (ECS B)

Computational design optimization overview

In a preliminary investigation stage, a series of experiments have been conducted, in order to find appropriate tools and methods for topology optimization analysis. Within this framework, the Millipede plug-in [31,32] for Grasshopper [34], has been tested, which focuses on the analysis and optimization of structures using a library for linear elastic systems analysis based on topology optimization [31]. The use of Millipede plug-in allows the development of integrated design optimization workflows, where optimization analysis and parametric design processes are bi-directionally related to each other.

Analytically, the following steps explain the topology optimization analysis undertaken in Millipede plug-in (Fig. 3): a. Firstly, by using closed solids, the boundaries of the systems' domain are defined, along with load regions, types of support as well as fixed density regions; b. Then, the Finite-Element Model is generated, where all the information from the previous components are aggregated. The resolution of the model, thus the size of cubic cells is being controlled in this stage; c. Next stage involves the topology optimization analysis. In this part of the process, parameters like the number of optimization iterations or target density are defined; d. Finally, analysis of results and their visualization are provided, which are derived from system's performance calculation. Among others, node results include displacement and volume elements results include principle stress, von Mises stress and material density. In terms of visualization, results include contours along surfaces of constant material density, ISO surface based on material distribution, stress lines, etc. In this initial experimentation, although the results calculated and produced by the solver are extractable for further investigation, only the visualization outputs of the ISO surface based material distribution are shown. In order to achieve this, the 3D-isoMesh component/command is used that generate contours along sur-

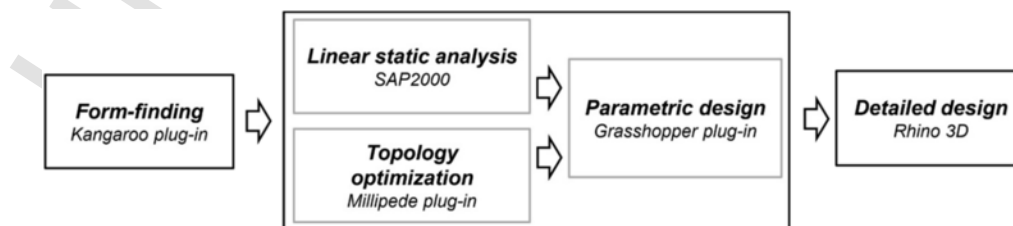


Fig. 2. Computational steps undertaken during optimization stage.

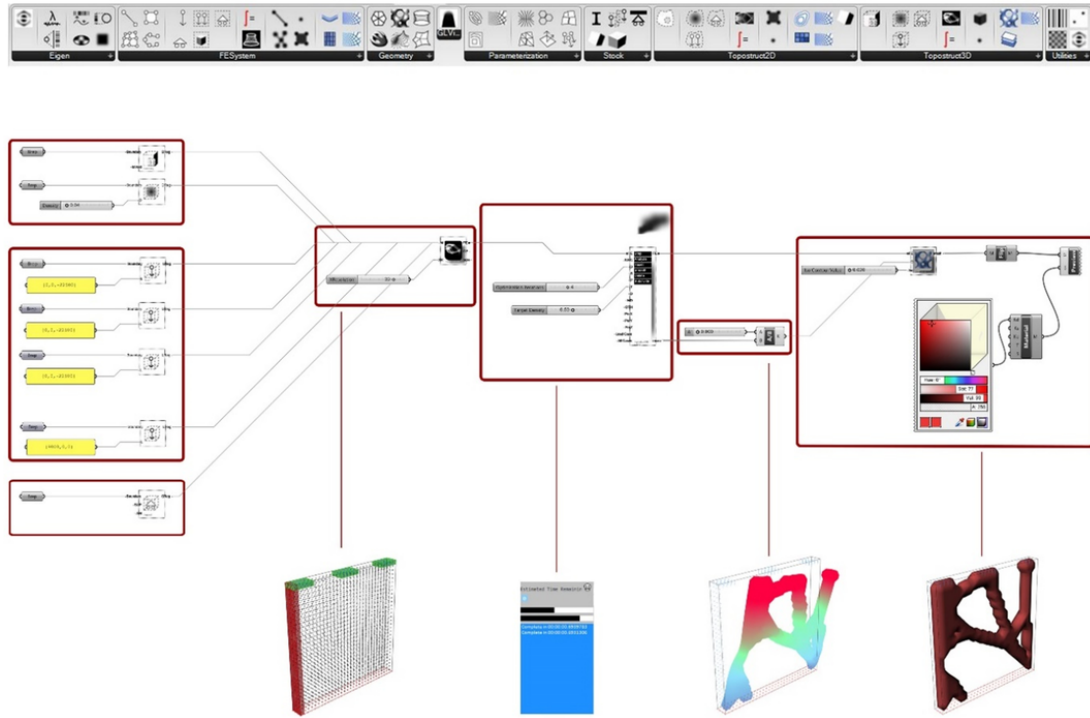


Fig. 3. Topology optimization analysis steps undertaken in Millipede plug-in.

face of constant material density. In this case, the input parameters include the FEM derived from the analysis, the Deflection factor (D) that is set to 0 and the Iso Contour value (Iso), which determines the density levels at which contours are drawn. In this case, the value is set to 0.02, which means that the contour that is generated separates material densities based on values less and larger than 0.02.

The tool is tested using as case study a shear wall (Fig. 4). In this initial experiment, the parameters considered to perform the optimization process are listed and explained as follows:

- The initial shear wall geometry where the optimization process is performed is represented by a box solid with boundary dimensions of $3.0 \times 3.0 \times 0.3 \text{ m}^3$ that is set from Rhino software. This is used as input for the component/command 3DBoundaryRegion.

- Fixed supports with fixed displacements and rotations where defined on the bottom of the wall element in the form of box solid using the component/command 3DSupportRegion.
- The load region is defined using the component/command 3DLoadRegion. This requires geometric inputs in the form of solids that are set again from Rhino software. In this case, vertical loads are applied on the top of the shear wall with maximum value 5 kN/m^3 . Horizontal load with maximum value 1 kN/m^2 is applied on the right edge of shear wall, again using as input a solid box.
- The creation of the Finite-Element Model (FEM) is achieved using the component/command Topostruct3DModel where all previous inputs of the model are assembled. In addition, the input XResolution (XR) determines the model resolution and specifically the number of cells

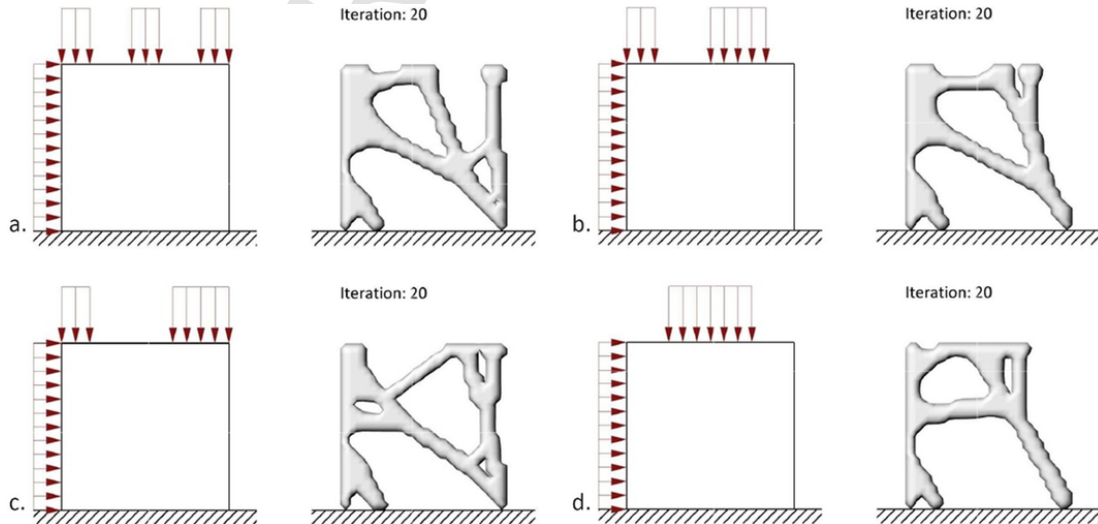


Fig. 4. Sample case studies of shear wall where topology optimization was tested. Constant horizontal load is applied while three vertical loads are combined in four combinations. a) 59% volume reduction; b) 61% volume reduction; c) 64% volume reduction; d) 69% volume reduction.

along the X direction. In this case, $XR = 30$ value is assigned, which is considered to be satisfactory providing that increased value requires longer computational time. Based on these input parameters, the FEM has resolution of 2700 voxels with individual dimensions of $0.1 \times 0.1 \times 0.1 \text{ m}^3$.

•The FEM analysis and topological optimization are performed using the component/command Topostruct3DSolver that represents the optimization solver of the Millipede plug-in. This command, apart from FEM input, contains a set of other input parameters that includes Self Weight Coefficient (SWC), Optimization iterations (O), Smoothing factor (S), Penalization factor (P), Target Density percentage (T), Initial Densities numbers (D), Minimum allowed density (MD), Delete Threshold value (DTH), Periodic in X, Y, and Z direction values (PerX & PerY & PerZ), Load Case number and All Cases Boolean input. In this example, the following input parameters are used:

- Optimization iterations (O) that defines the number of iterations performed by the solver. For the experiments shown in Fig. 4, the O input is set to 20 iterations, though this number can be different in order for the morphology to be stabilized depending on the complexity of each case under investigation.
- Smoothing factor (S) between 0.0 (no smoothing) and 1.0 can be applied to each iteration to avoid the generation of checker patterns. In this case the number is set to 0.1.
- Penalization factor (P) that defines the steps needed the optimization to converge to a black and white state. A larger number means fewer steps however this might fail to redistribute material properly and for this reason a value from 1.5 to 3.0 is recommended by the developers (Millipede plug-in manual). In this case P input is set to 3.0.
- Target Density (T) that determines the percentage of the fraction of the overall material remaining after optimization is performed in the form of a number from 0.0 to 1.0. In this case the T input is set to 0.5.
- Minimum allowed density (MD) that defines the minimum density of elements, which is recommended by the developers to be from 0.01 to 0.001. In this case the value is set to 0.001.
- Delete Threshold value (DTH) that defines the density value below which all quads are eliminated for speeding up further steps purposes and in this case is set to 0.5.

Nodes topology optimization and members' standardization (ECS A)

As already mentioned, in ECS A, the approach has been concentrated on the topology optimization of nodes and the standardization of structural members of the shell structure. In order to achieve this, a simple free-form shell structure has been generated and tessellated with hexagons, by projecting a flat hexagonal grid (on the XY-axis) over the initial surface of the structure. Then, by using FEA, the axial forces on the position of the nodes' hexagonal grid have been calculated. Subsequently, the forces acting on each node have been used in the process of topology optimization in Millipede plug-in. The results provided custom and non-regular morphologies on each node position, that were fabricated in considering the sustainability aspect of the fabrication process involved (Fig. 5).

The design optimization process based on the topological development of nodes leads to morphological results with highly fluctuated and non-standard shapes, which can be characterized as one-of solutions. This means that during the physical production, as many procedures as the number of nodes should be developed. This raises several issues in terms of the effectiveness of the fabrication process to be applied, in order to be characterized as a feasible procedure for the construction of free-form shell structures in actual scale.

Members' topology optimization and nodes standardization (ECS B)

In ECS B, the process follows a different direction, that is the application of topology optimization principles on the shell's structural member, while the development of nodes follows a standardized mass production process. Initially, as in the previous ECS, the overall shell geometry and its tessellation are defined. In order to achieve this, the Kangaroo physics engine (plug-in for Grasshopper) is applied for the shell's overall form-finding by defining four curves under bending forces, whereas a respective number of anchor points at their ends can be moved to deform the overall surface. Then, surface discretization is achieved by using a 7×11 grid of $0.75 \times 0.75 \text{ m}^2$ square cells. The surface is divided into squares, using the Lunchbox plug-in [59] for Grasshopper.

Within this context, a variety of parametrically controlled morphologies can be derived. The different hypothesis that caused surface deformations produced are based on geometrical criteria related to the height and area of space in order to accommodate one or more users. In addition, an extra constraint has been to maintain shape differentiation of units as low as possible for minimization the variability of re-

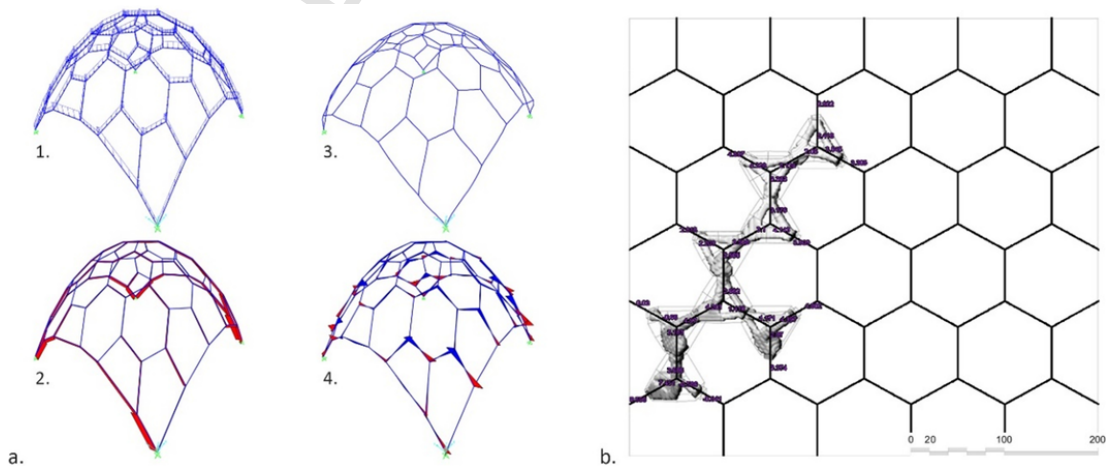


Fig. 5. Nodes' topology optimization process. a) Structural behaviour under vertical loading. a1) Structural system; a2) Axial forces diagram; a3) Vertical deformation; a4) Bending moments diagram. b) Results of optimization in every node based on axial forces derived from FEA analysis.

configurable mechanism. For this reason, minimum deviations of unit structures' spans in both surface directions are aimed at. Results of this process, shows similarities in terms of their composing quadrangles' edges length that are ensured within $\pm 0.03\text{m}$ divergence from their initial 0.75m dimension. This gives a first inside on the ability of the specific tessellation technique and hence, of the results obtained to allow easy fabrication of individual structural members at the construction stage. Fig. 6 shows the parametric and physics-based generation process of the overall shell geometry, together with a number of possible results of surface deformation. In each surface the range of quadrangles' edges dimensions is also demonstrated.

Then, four results are selected based on the criterion of minimum deviations of unit structures' spans in both surface directions (Fig. 7). These results contain symmetrical and non-symmetrical features and include a simple rectangle, right trapezoid, parallelogram and isosceles trapezoid in XY-plan. Subsequently, the selected surfaces are offset, creating 0.15m thick shell systems. Their topology optimization process together with their load-deformation behaviour, follow the settings provided in the initial part of this sub-section. Specifically, the poly-surface is divided into voxels with dimensions 0.075m that constitutes the domain of the topology optimization algorithm. Then, the support and load areas are defined and a Finite-Element Model is developed. The topology optimization process is set to run twelve iterations and the target density is set to 0.2 , which, after several tests and density's differentiations ranging from 0.0 to 1.0 , has showed, together with target density value of 0.5 , that is the most appropriate value to be used

in order to ensure satisfactory results of material density distribution, while serving the volume reduction targets initially set. As output data, values for the principle stresses, von Mises stresses and material densities are extracted for each voxel of the system. These values are then visualized based on the given voxels. The density values are visualized by applying a box in each voxel that is modified proportionally, while the colour range from light red to dark red shows proportionally variations of the material density after the shell structure is topologically optimized (Fig. 8).

The structure has been analysed with the Finite-Element software program SAP2000. The nonlinear analysis of the system was based on a respective node and member 3-D model. Each of the 308 Y-shaped units consists of three rigidly connected members with respective rectangular r/c sections of $t_1 = 15\text{cm}$, $t_2 = 10\text{cm}$ that define their respective height and width. Two longitudinal bars of diameter $\varnothing 8\text{mm}$ were defined as reinforcement of the sections, and confinement bars of diameter $\varnothing 6\text{mm}$ were placed at equal length intervals of 15cm . Concrete C20/25 was used with mixture ratio to be water 0.5 , Portland cement 1.0 , sand 2.0 and aggregates 4.0 . The Y-shaped units interconnections and the systems ground supports are moment-free. The structural analysis conducted considered the self-weight of the structure and a uniform distributed vertical loading of the members of 0.5kN/m , further increased by a safety factor of 1.35 . The results obtained are shown in Fig. 9. The maximum axial forces of the members amount to 50.9kN and 31.9kN developed in the rear base and front upper members of the system respectively. The maximum bending moment

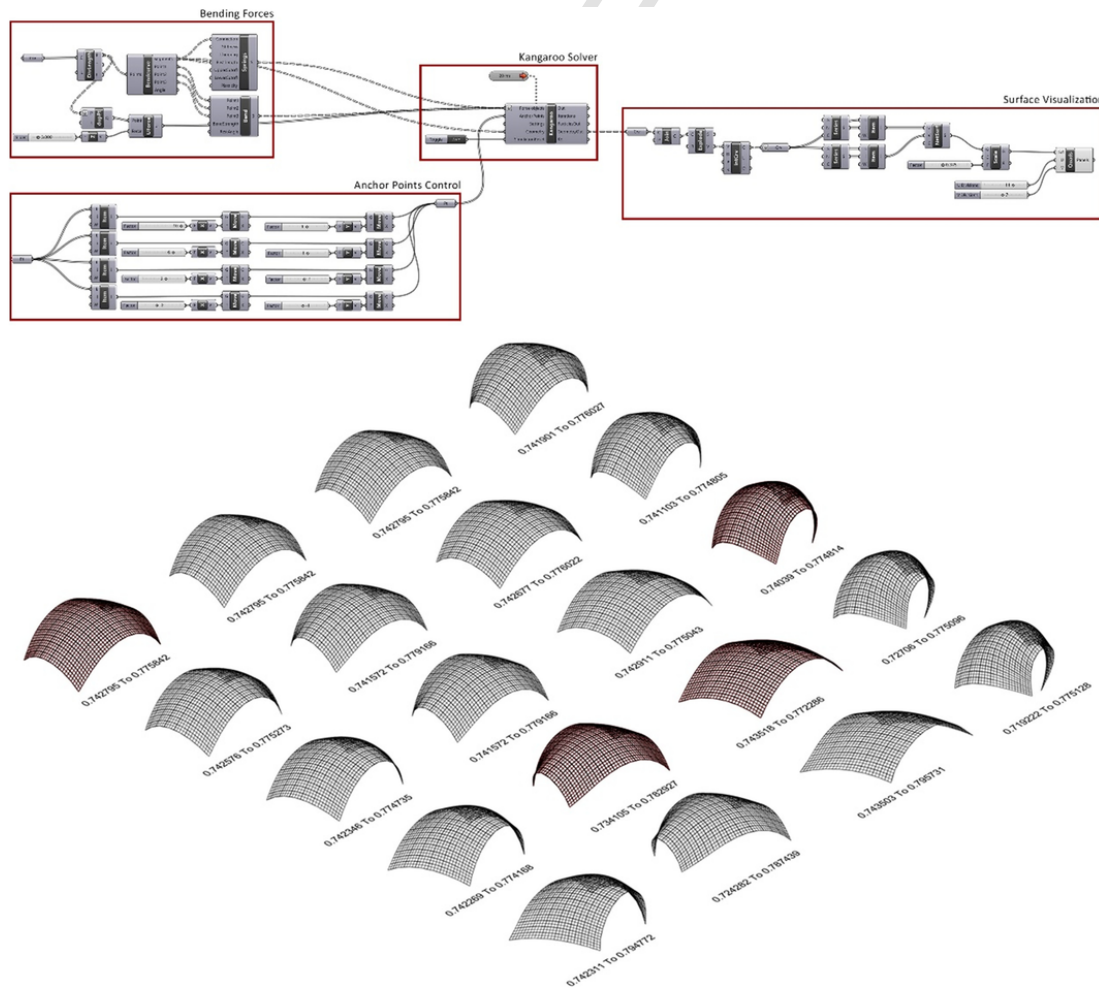


Fig. 6. Parametric generation of the overall shell geometry and tessellation process.

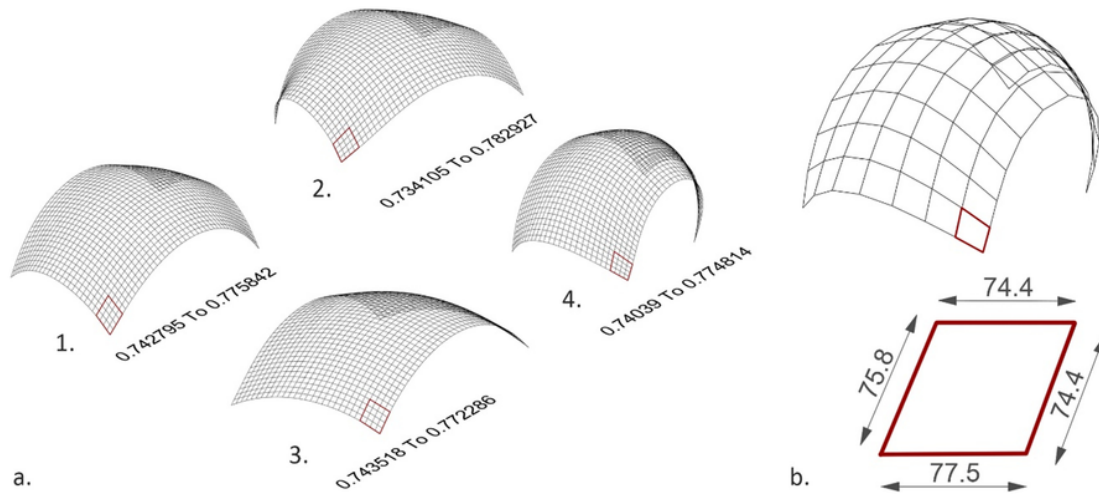


Fig. 7. a) Four selected results of shell geometry with the minimum deviations of unit structures' spans in both surface directions. a1) Plan area: 34.51 m²; Height: 2.93 m; Max arc: 2.24 m; Min arc: 1.2 m. a2) Plan area: 33.15 m²; Height: 2.97 m; Max arc: 2.19 m; Min arc: 1.2 m. a3) Plan area: 30.92 m²; Height: 2.84 m; Max arc: 2.23 m; Min arc: 0.82 m. a4) Plan area: 25.30 m²; Height: 3.81 m; Max arc: 3.39 m; Min arc: 1.28 m. b) Selected geometry d for further investigation. Individual cell where deviations of cells structures' spans in both surface directions is demonstrated.

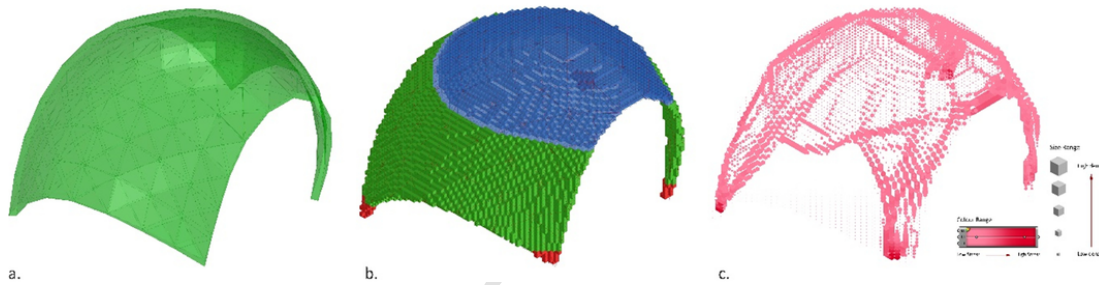


Fig. 8. Topology optimization and initial results. a) The boundary geometry where optimization takes place. b) The vertical loads in blue and supports in red. c) Visual representation of optimization process: The voxels are scaled down respectively to their new density. (For interpretation of the references to colour in this figure legend, the reader is referred to the web version of this article.)

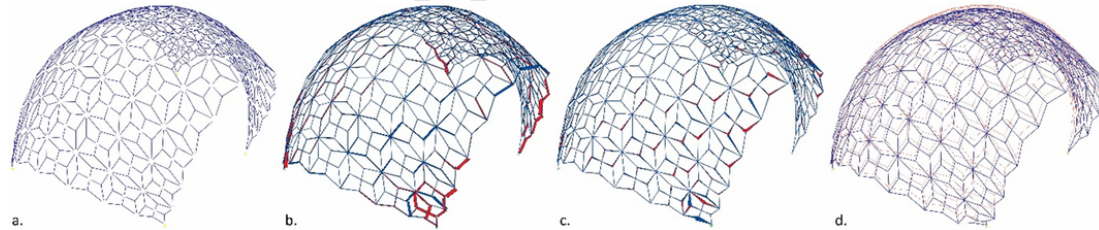


Fig. 9. Structural behaviour under vertical loading. a) Structural system; b) Axial forces diagram; c) Bending moments diagram; d) Vertical deformation.

amounts to 5.38 kNm developed in the front base units, and the maximum vertical deformation of the structure amounts to 1.3 cm. In the structural analysis, no buckling of the members has been considered.

Topology optimization has been applied in the selected four shell structures (Fig. 7), displaying how the algorithms affect every structure in terms of material density (Fig. 10). The results derived from topology optimization are then visualized according to the predefined shell voxels. Moreover, the proportional deformation of individual structural unit members (analytical explanation on shape formation is given in the following sub-section) according to the material density derived from the optimization shows the distribution of the elements' thickness and hence the final results obtained (Fig. 11). This gives a first insight into how the structural units are alternated corresponding to the suggested topology optimization analysis process. In all cases, the process of adapting the structural units' sections to the free-form shell according to the results of topology optimization enables a reduction in the total shell volume from 6.23 m³ to 2.16 m³ on average, indicating

that the process can achieve minimization of mass used for fabrication of up to 65.3% compared to the conventional evenly distributed thickness of the shell.

Shape formation of structural unit members using topology optimization

The process of shaping and alternation of individual unit members is based on the varying results of material density that have been derived from topology optimization. Towards this direction, the initial quadrat units used in the optimization stage are divided into 308 triangular ones that enclose a selected Y-shape as the final geometry of each structural member. The choice of this shape was made because of its ability to create rigid triangular planes that can be easily assembled in the overall system in combination of 4 and 8 joints. Also, because of the possibility of alternate its shape by varying the thickness of its three contained wings, offering numerous possibilities of structural variations based on the material density values at each location of the unit within

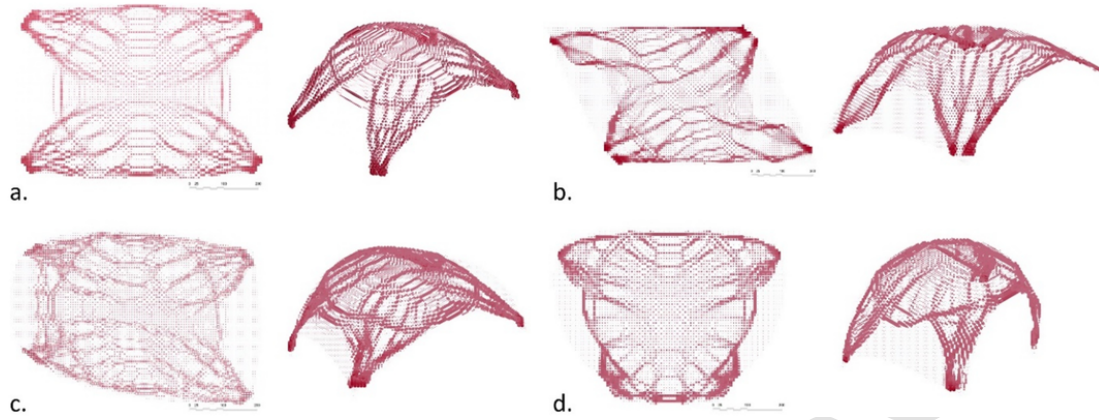


Fig. 10. Visualization of topology optimization results for the four selected shell structures a, b, c, and d. The voxels are scaled down respectively to their new density.

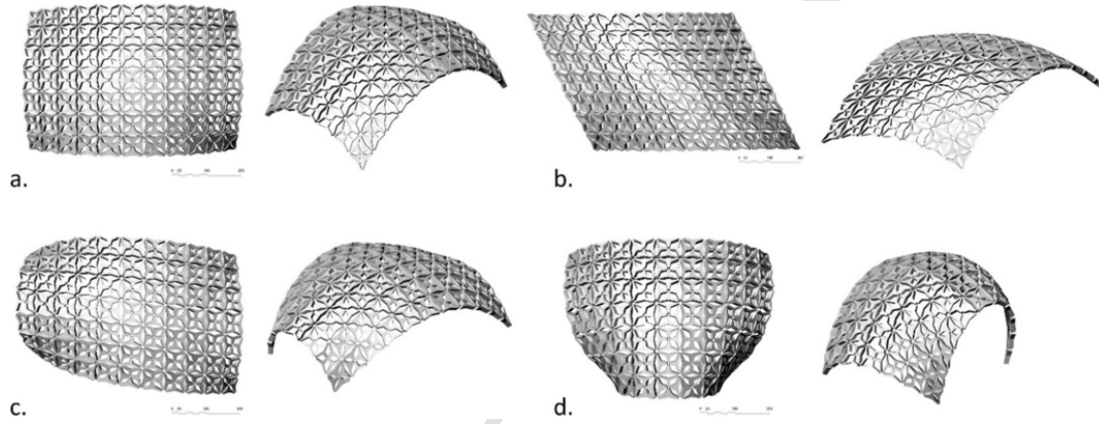


Fig. 11. Deformation of individual structural units and final results of shell structures a, b, c, and d.

the shell system. All the above are coupled with the possibility of developing a reconfigurable formwork which can provide an effective production of the units.

Fig. 12 shows a schematic relation between the results of topology optimization and the Y-shape formation. The average material density based on the FEA as derived from the optimization, refers to numeric values from 0.001 to 1. These values are responsible for further trans-

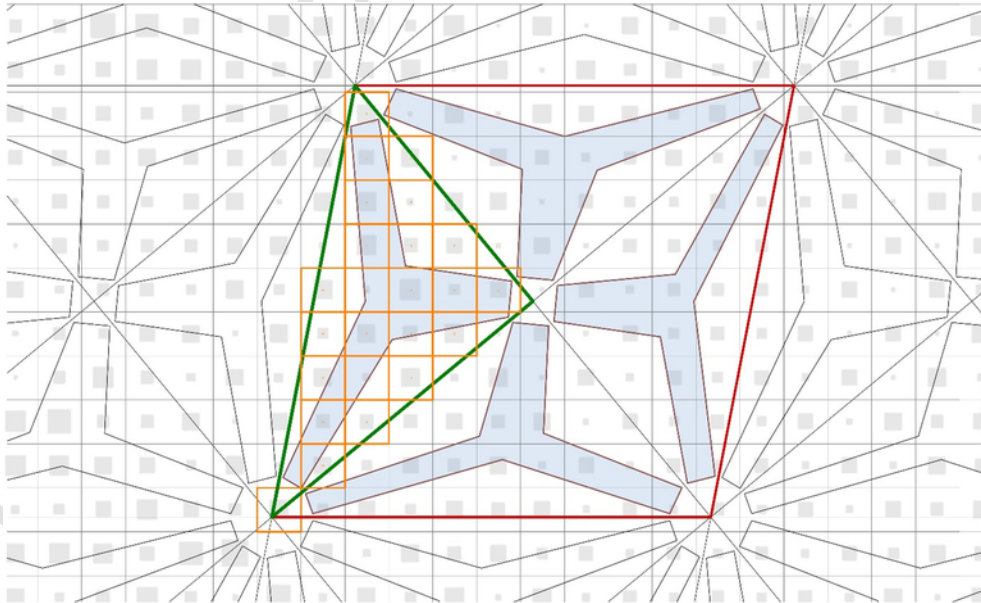


Fig. 12. Each voxel gets a density value from the optimization process between 0.001 and 1. For each unit (green outline) the average density of the contained voxels is calculated (orange outline), which afterwards is responsible for the plan deformation of the unit. With red the quadrangle that includes 4 units with their respective average density, which is responsible for the section deformation. (For interpretation of the references to colour in this figure legend, the reader is referred to the web version of this article.)

formation of the units, both in plan and in section based on a number of geometrically transformed parameters that are connected with the reconfigurable behaviour of the formwork (Figs. 14 and 15).

Specifically, the plan volume reduction (Remap-P) starts by determining the geometry of each triangle based on its position to the shell. This is a Y-shape that is enclosed in a rectangle ADB with hypotenuse (AB) equal to 75 cm. Based on this, the D corner is allowed to slide over the semicircle formed by the points A, D, and B. Also, on the same triangle the lines L1, L2, and L3 are defined from the centroid of the triangle to the midpoint of triangle sides M1, M2, and M3, respectively. Over their length, the position of the inside corners of each Y-shape is evaluated based on the distances R1, R2, and R3 and is determined according to the results of Remap-P, which accepts average material den-

sity values of corresponding units and remaps their distances (R1, R2, and R3) in the range of 25%–75% of the initial L1, L2, and L3 respectively. R values are restrained within Rmin and Rmax constant values ranged from 10 to 14 cm. The final Y-shape is formulated based on the position of these new corners and the ones that result from the intersection of t-offsets (0.6 cm) as well as from the corners produced by the intersection of arcs in A, B, and D initial triangle corners with radiuses d1 (7 cm) and d2 (5 cm) respectively (Fig. 13-a).

The plan volume reduction is followed by the section volume reduction (Remap-S). In this case, a new average density is calculated for each quad-unit group of 4 triangles. These values are then remapped to determine the vertical height of point D (h), that together with the AB edge define the slicing plane that trims the Y-shape, reducing its vol-

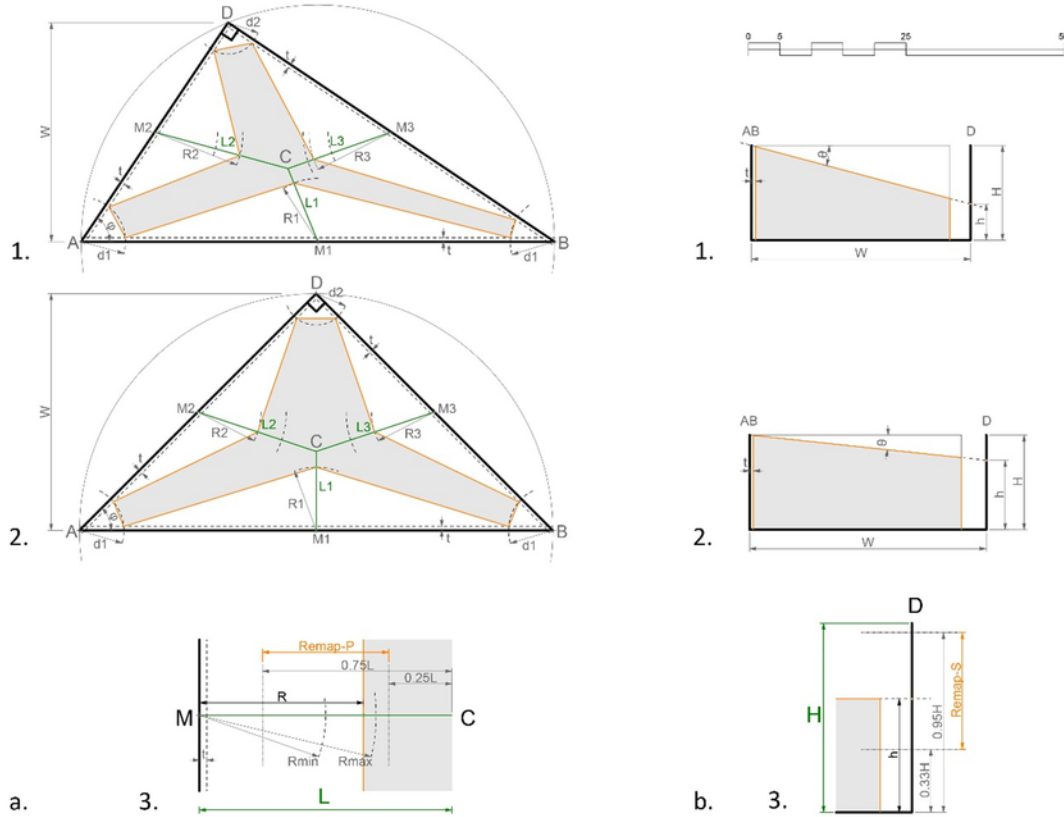


Fig. 13. a) The geometric transformation of two units in plan, illustrating how the geometry of ADB triangle and the Remap values affect the final Y-shape geometry. a1) The lowest volume unit (no. 7). a2) The highest volume unit (no. 140). a3) Diagrammatic representation of the average density values and their influence on the geometric alternations of units in plan. Remap-P values control R lengths over L lines. b) The geometric transformation of the same units no.7 (b1) and no. 140 (b2) in section. b3) Remap-S values control h length over H height.

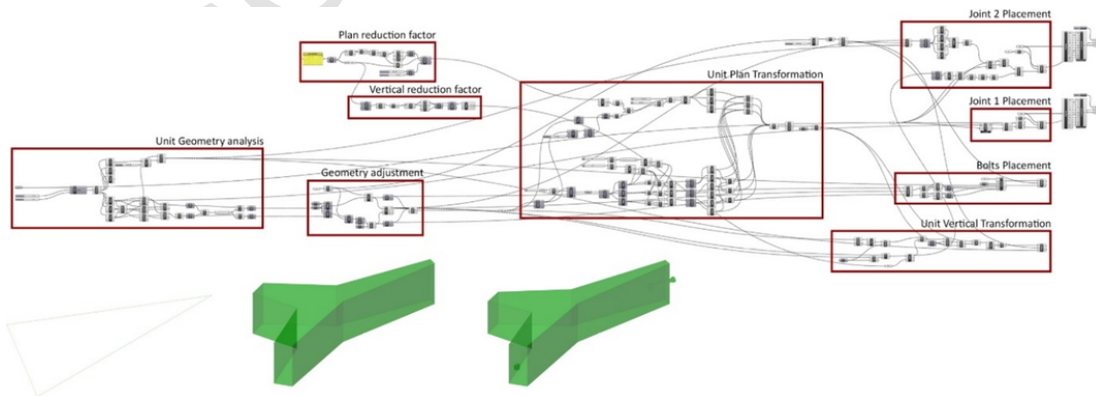


Fig. 14. Parametric design and control algorithm of the structural unit.

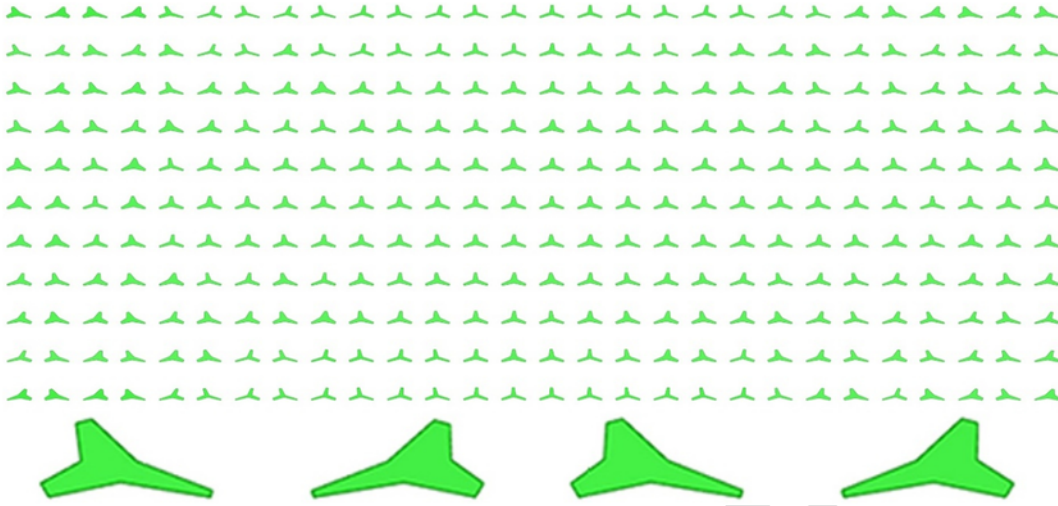


Fig. 15. Structural units in 308 variations.

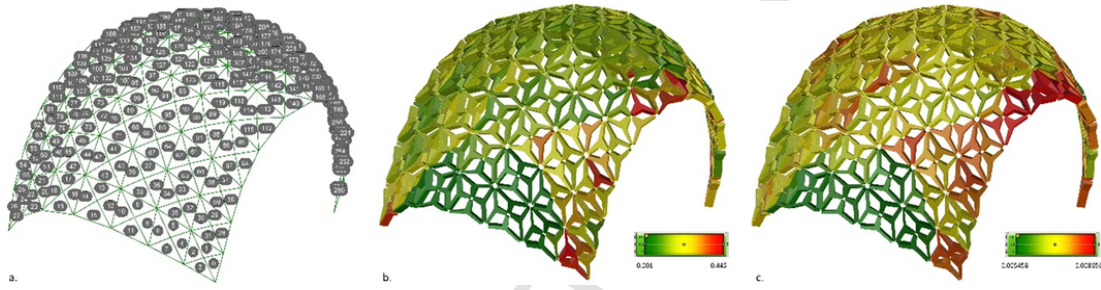


Fig. 16. a) Units' numbering. b) Colouring of the units according to their average density. Green is 0.001 and red is 0.445. c) Colouring of the units according to their final volume. Green is 0.005458m³ and red is 0.008656m³. (For interpretation of the references to colour in this figure legend, the reader is referred to the web version of this article.)



Fig. 17. a) The relation between the average densities that derived from the optimization process and the final volumes for each unit. b) The initial triangle volume, the volume after the deformation in plan and the final volume after the reduction for each unit in plan.

ume in section. Specifically, the height h on the triangle corner D accepts values between 33% - 95% of the initial height H (15 cm) of the volume, depending on the results of Remap-S for respective Y-shape units. Within the quad-units group, value h is the same. Thus, angle θ determined from the slicing and initial triangle ADB planes depends on the values h and distance W (Fig. 13-b).

Fig. 16 demonstrate the distribution of alternate units on the shell structure according to the range of material densities and Fig. 17 the relation between average density and volumes of each unit (Fig. 17-a) as well as the relation between initial, final and volume reduction in plan (Fig. 17-b).

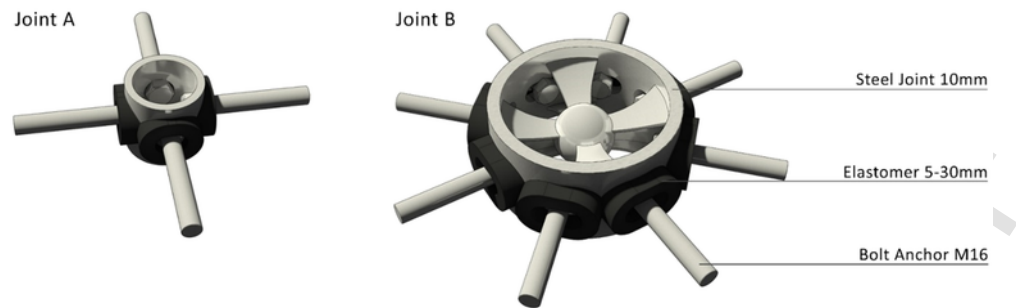


Fig. 18. Two types of joints. Left: Joint A, Right: Joint B.

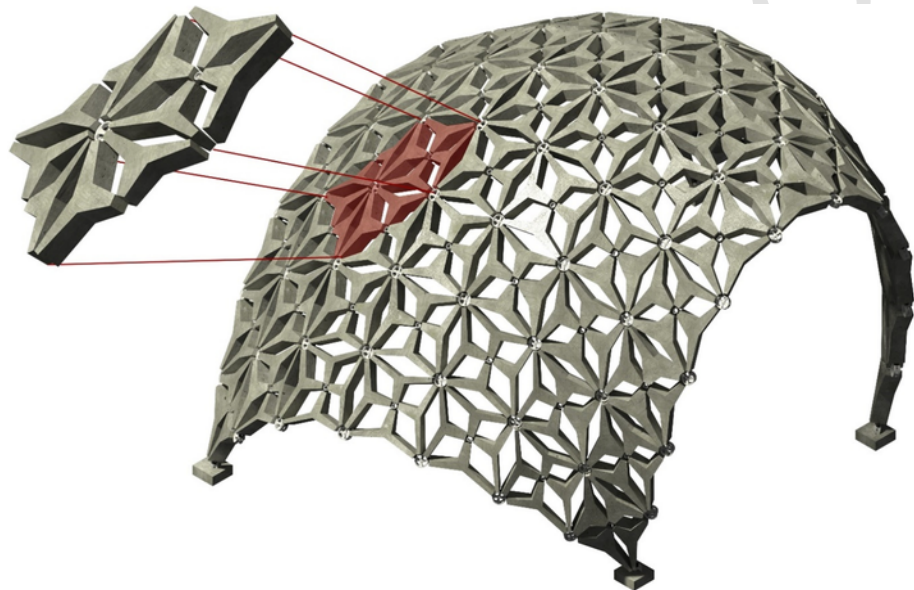


Fig. 19. Overall shell structure and embodiment of joints to capture its curved shape.

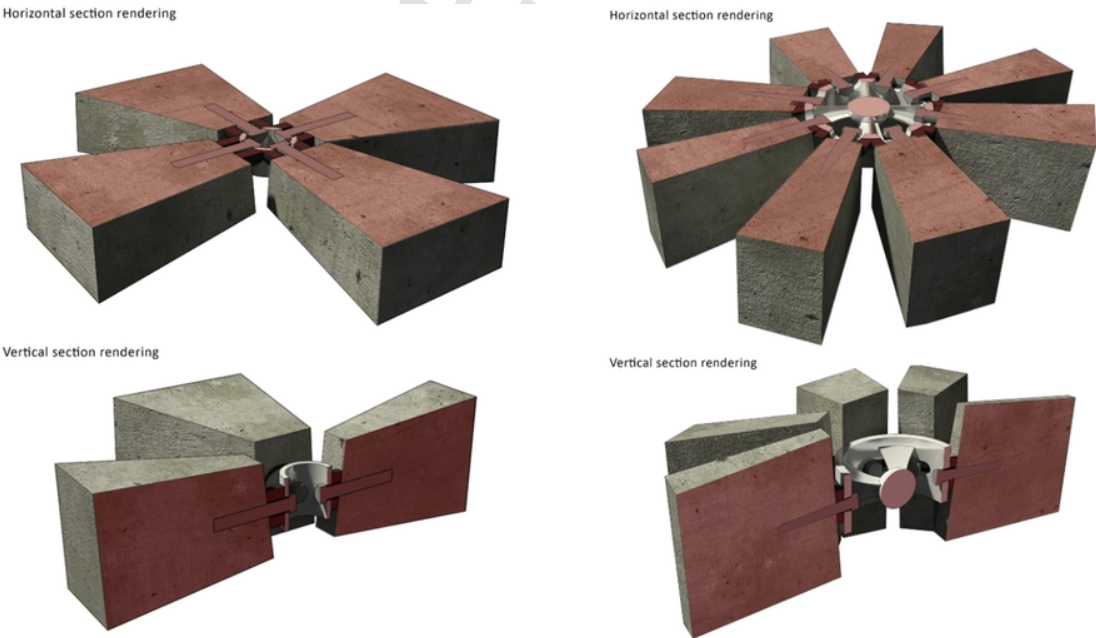


Fig. 20. Detailed design of Joint A and Joint B.

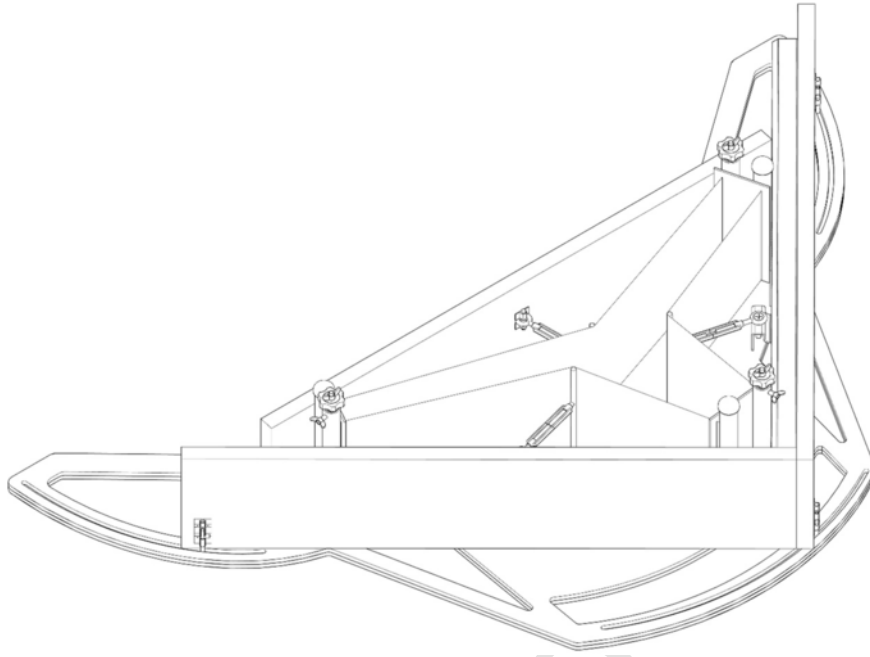


Fig. 21. Axonometric view of the reconfigurable formwork mechanism and possible movement of parts.

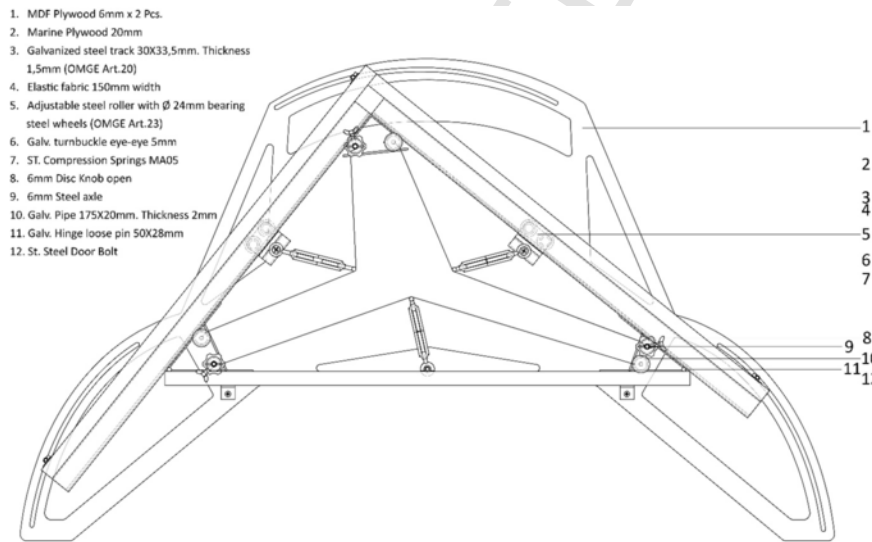


Fig. 22. Detailed drawing of the mechanism and included parts.

Detailed design development

The steel fibre-reinforced concrete modules' shape changes according to the results obtained from the topology optimization analysis, where more mass is placed to the elements with higher density values. The design of joints that connect the units together, complete the suggested design development of the shell. Two types of standardized, prefabricated joints are required: one that connects four Y-shaped units (Joint A) and one that connects eight Y-shaped units together (Joint B). Bolt anchors [60] are embodied on each end of the units that allow 16M bolts to screw the joints on them (Fig. 18). In structural terms, the joint connections to the units are moment-free. By further respective demand for semi-rigid connections, this may be achieved with double bolt anchors over the height of the connecting joints with the unit sections. In all cases, the joints allow the units to be hooked in multiple angles, in following the overall curved shape of the structure (Fig. 19).

Different connection angles of the members to the joints and the deviations between the units are made possible with the use of elastomer sheets of varying thickness between 5 and 30 mm (Fig. 20). The thickness of the elastomer sheet has been determined based on the maximum axial force developed in the respective connected member. Based on the assumed external vertical loading of the structure, the deformation of the elastomer is within the required limits.

Reconfigurable kinetic formwork development

Despite their vast use in the building industry, materials like cement, plaster and clay are not so widespread in digital fabrication, due to mechanical limitations. Mass-customized moulds are commonly used in such cases, but waste material and cost comprise constraining factors, making their widespread use in construction industry non-profitable. However, material waste can be reduced, by using adaptive fabrication techniques, which can be promising, provided that integration

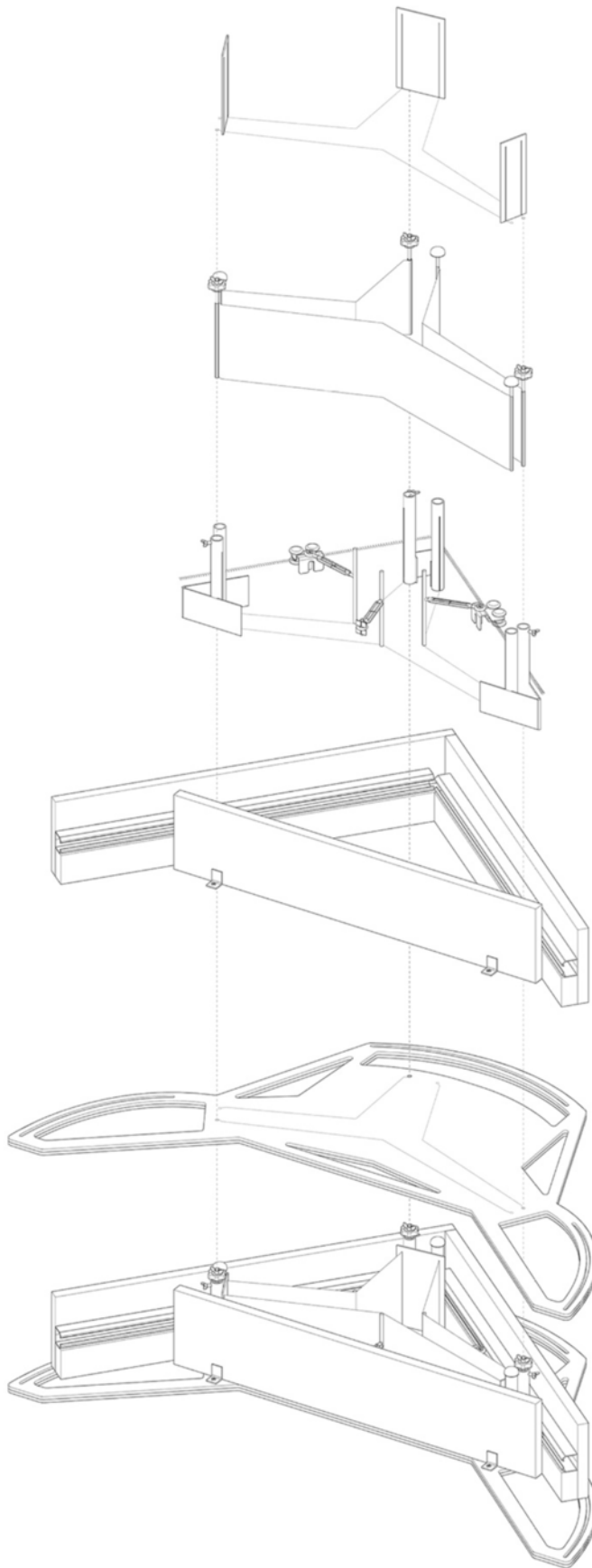


Fig. 23. Parts of reconfigurable formwork mechanism.



with computational design processes are established, influencing decisions taken in the design development stage and vice versa.

Design development and details of reconfigurable formwork

In this project, the reconfigurable formwork introduced, allows its reusability, due to the benefits of applying the same adaptive principles to fabricate all custom modules of the given shell structure, achieving in parallel, minimization of material consumption. Analytically, the morphological versatility of modules is captured during the fabrication stage by developing and operating a semi-automated reconfigurable formwork, which is capable to adjust its shape according to different module sections. The reconfigurable mechanism has been designed to receive the Y-shape of the modules and any of their deviations needed. The mechanism is able to adjust its form according to each proportion of modular structural element, by dragging the adjacent sides of the right triangle along the hypotenuse (Fig. 21). The motion on the mechanism is achieved by three engraved tracks on the mechanism's base (Fig. 22-1), where the moving parts drag over them. Simultaneously, the midpoint of each side of the base triangle is found automatically, through the modified use of a door sliding system (Fig. 22-3,5) in combination with compression springs (Fig. 22-7). On those midpoints, turnbuckles (Fig. 22-6) are adapted, which can extend as desired, and hold vertical bars. Three flexible membranes (Fig. 22-4) formulate the final unit's shape, when wrapped around the bars. The units are enclosed with the addition of custom Medium-Density Fibreboards (MDF) plates that are placed at the ends, between the membranes (Fig. 23).

Also, the reconfigurable formwork can be rotated on the horizontal axis, which passes through the hypotenuse, 'slicing' in this way the unit in section. After demoulding of each modular structural element, the formwork can be adapted to the next modular geometry until all elements are produced. Fig. 24 shows the procedure of developing and adjusting the mechanism. This requires slicing, welding, abrasion, gluing, drilling and fixing. Table 1 demonstrates the time needed for the development of the formwork prototype and subsequent series production. While in the first case, the time needed to fabricate the formwork amounts 35 h, in the second case it assumed that in the frame of the series of production of the formwork and assembly, the formwork unit would amount approximately 8 h. Table 2 shows the materials used and the total cost of prototype formwork development.

Operation

In order to reconfigure the geometry of the formwork according to the shape under construction, a specific procedure is followed:

- First, the membranes and then the turnbuckles need to be relaxed.
- Subsequently, the right angle should slide around the hypotenuse to adjust its new position.
- Then, turning the turnbuckles, the membranes adjust to the new unit's geometry, where they tighten on place.
- Finally, the MDF plates are placed in the inner part of the mould and the formwork is ready to be casted.

Fig. 25 displays four different cases of readjusting the suggested reconfigurable mechanism, demonstrating in parallel its functionality. The reconfigurable mechanism was developed and tested with encouraging results. The system has the potential to be robotically controlled with further modifications.



Fig. 24. Procedure of developing the parts and adjusting the mechanism.



Fig. 25. Readjustment of reconfigurable mechanism.

Sample prototyping

In order to demonstrate the functionality of the reconfigurable mechanism, initially a gypsum module has been constructed. The initial preparations included spraying the surfaces with releasing oil and checking everything to be fixed. Then, the gypsum is mixed with water and casted in the mould carefully, not to be spelt over the membranes. The tilt needed was also given to the mechanism, so that the resulting model has the indicated reduction in section. After a certain hardening time period, the membranes and the turnbuckles are relaxed and the model is carefully demoulded. Finally, the mechanism is prepared to adapt its shape and be casted according to the next module's geometry (Fig. 26).

Physical prototyping results

The suggested design has been developed, in order to test the feasibility of design and semi-automated construction methodology described in the previous sections. Analytically, the shell structure investigated is a trapezoid in plan, covering an area of $5 \times 6.5\text{m}$, with maximum height of 3.85m . The height of the front arch is 3.35m , the rear, 2.50m , and the sides, 1.30m . The prototype is composed of 308 unique concrete Y-shaped units, which are produced using the suggested reconfigurable formwork mechanism, intergrading at the same time anchor bolts, in order to attach the units on each steel joints. Furthermore, 77 joints of type A and 92 joints of type B are used for the development of the structure, which are responsible for its curvature and stability (Fig. 27). A physical prototype of four modules was built that

served as initial proof-of-concept. The following sub-sections describe the process of physical production and adjustment of four interconnected structural elements.

Formwork preparation

After having selected the modules to be casted (Fig. 28), the reconfigurable formwork has been readjusted to capture the geometry of the selected customized structural elements. Towards this direction, the three node-points of the unit, as well as the three mid-points of edges are used to adjust the geometrical configuration of the unit, modifying the whole system accordingly. Subsequently, the membrane has been tested and pieces of plywood were placed on the three corners. After spraying the formwork, the mould was ready for casting. Also, the anchor bolts were added to the formwork, which act as reinforced steel members and extensions of the units for the respective interconnections (Fig. 29).

Concrete casting and demoulding

The formwork preparation is followed by the concrete mixture creation. At the design analysis level, the reinforced concrete used for the units has been defined as C20/25 (See Section 3.3). However, the construction experiments described in this paper focus more on the effectiveness of the construction process as a whole and not specifically on mixture composition and material use. Future research will give more emphasis on the consistency of the mixture, which can be characterized as a construction aspect, equally important to other aspects considered with regard to the physical results obtained. Table 3 includes the ma-

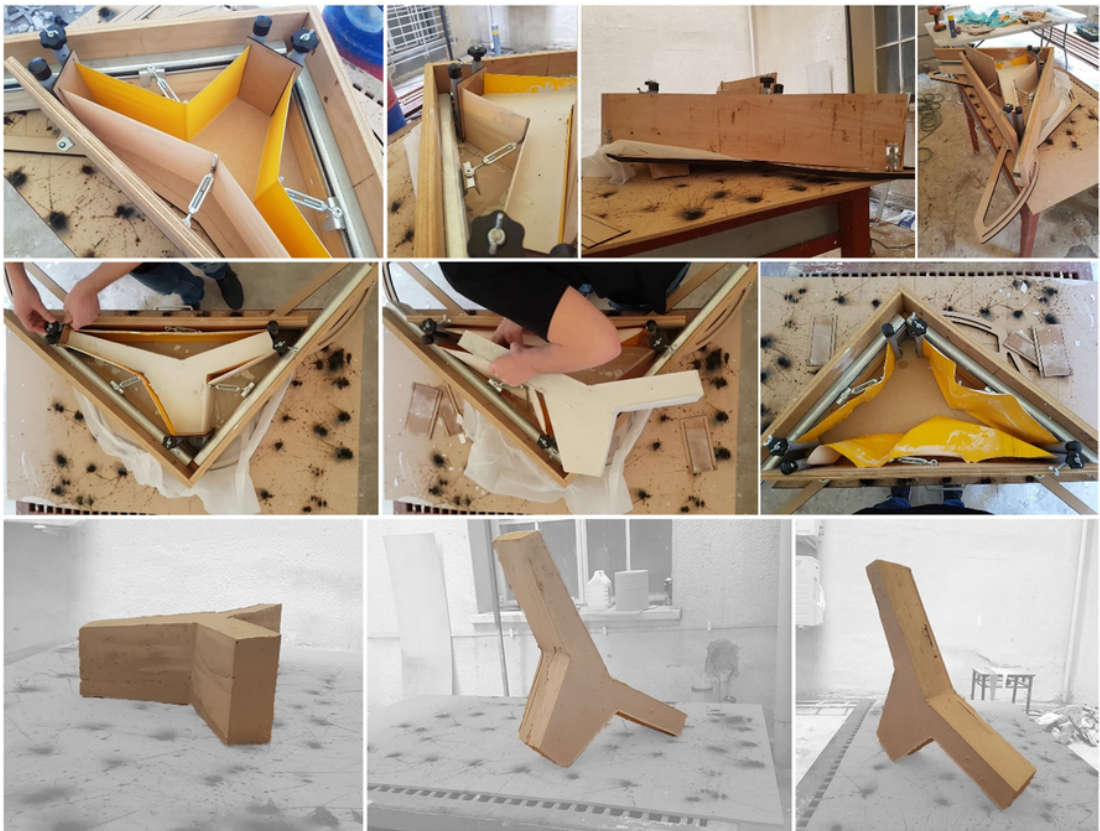


Fig. 26. The process of sample prototyping using the reconfigurable mechanism.

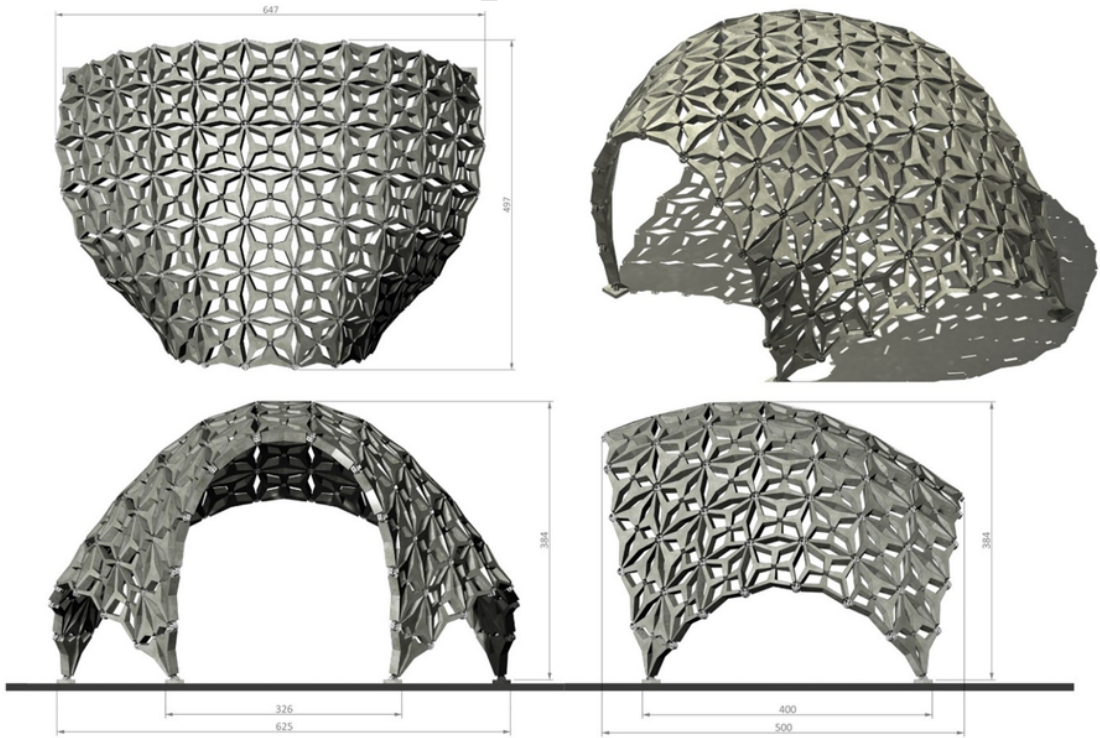


Fig. 27. Selected case study of free-form shell structure for prototyping.

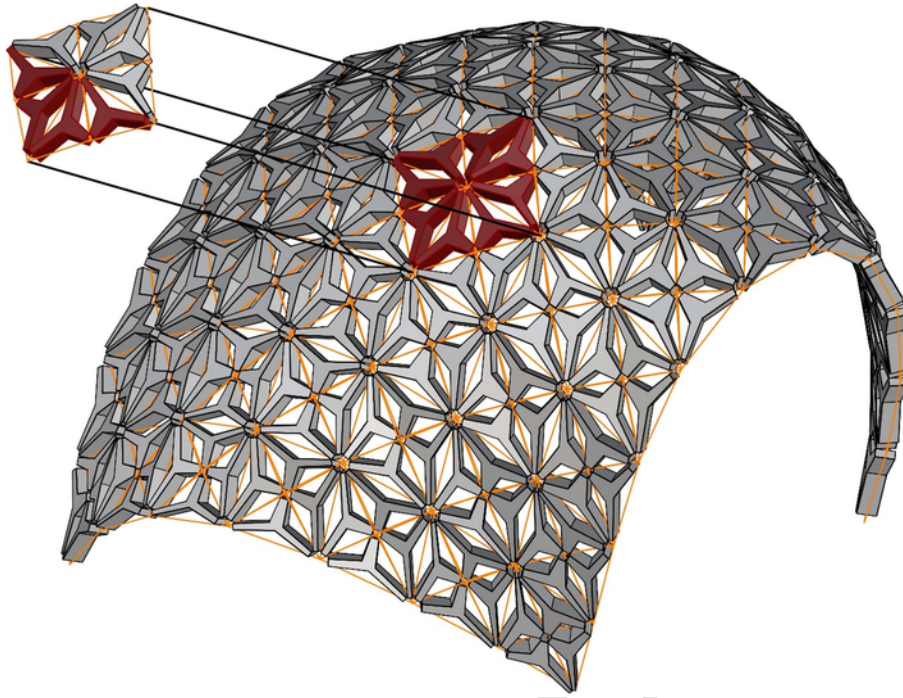


Fig. 28. Selected modules for physical prototyping.



Fig. 29. Formwork preparation for casting.

terial proportions by weight included in the mixture used in the case study.

Following the concrete casting, which together with the concrete material preparation lasted 20 min in total, and 22.5 h of concrete curing, each unit is ready for demoulding. The timetable for constructing of a custom structural element can be found in Table 4. The formwork preparation, the concrete mixture creation and casting, as well as the

demoulding process took approximately 24 h in total and involved one skilled labor. The operation has been repeated five times according to the number of units produced. Table 4 presents the activities and the time needed respectively for the physical prototype development.



Fig. 30. Formwork preparation, casting and curing activities.



Fig. 31. Four structural modular elements assembly.

Manufacturing and assembly

The suggested comprehensive construction of free-form shell structure driven by the reconfigurable formwork is based on a precast construction method, which shows a number of advantages in regard to the cast-in place method. This include among others better quality of produced concrete elements due to the inspection of material occurring in the ground, better geometrical compatibility, proper connection of modules and reduced material formwork cost [61]. In this paper, the suggested comprehensive construction combines precast method with cast-in place methods, mainly for the application of supporting system of scaffoldings during erection. This can be done with the use of minimum possible materials either steel or timber structure that can support the shell morphology in specific locations [62].

The suggested overall assembly process is based on a successive addition of elements [63] that requires the formulation of initial arches with fixed support points to the ground. Then, shell's surface regions, which are enclosed within the arches are filled with modules to achieve the stability of the overall structure and are strengthened by minimum supporting system that consists of long shores and bracing systems. In order to test the suggested process and to indicate how the units can be adjusted together for the development of the entire structure with future objective the demonstration of a comprehensive assembly process, this sections describes a series of steps using a prototype of four structural elements (See Fig. 28). Fig. 30 shows selective steps during the

manufacturing process of four structural modular elements. The formwork, as it appears after the preparation, is shown together with the casting and curing process. Then, the assembly process of four elements is demonstrated in Fig. 31. Fig. 32 shows the prototype of four structural modular elements adjusted together by using two types of joints.

Estimation of cost and fabrication time

The estimation of cost and time of fabrication of the suggested reconfigurable formwork as well as comparison with conventional formworks has been conducted, by deriving data from the local construction industry. For comparative purposes, the same modular component of structure has been used as the case study for formwork analysis (Fig. 33). Due to the difficulties in finding corresponding data in local industry, this has been done through personal communication with contractors and labors. The investigation takes place at the formwork level and does not include assembly and erection costs. Table 5 and Table 6 show results of fabrication cost for the conventional and for the reconfigurable formwork respectively. Table 7 and Table 8 demonstrate results of fabrication time for the conventional and the reconfigurable formwork respectively. Finally, Table 9 shows a comparison that includes working days for conventional and reconfigurable formwork fabrication and concrete curing time.

Results show that the fabrication cost of reconfigurable formwork is considerably less than the fabrication cost of conventional formwork. Also, the fabrication time of conventional formwork is approximately

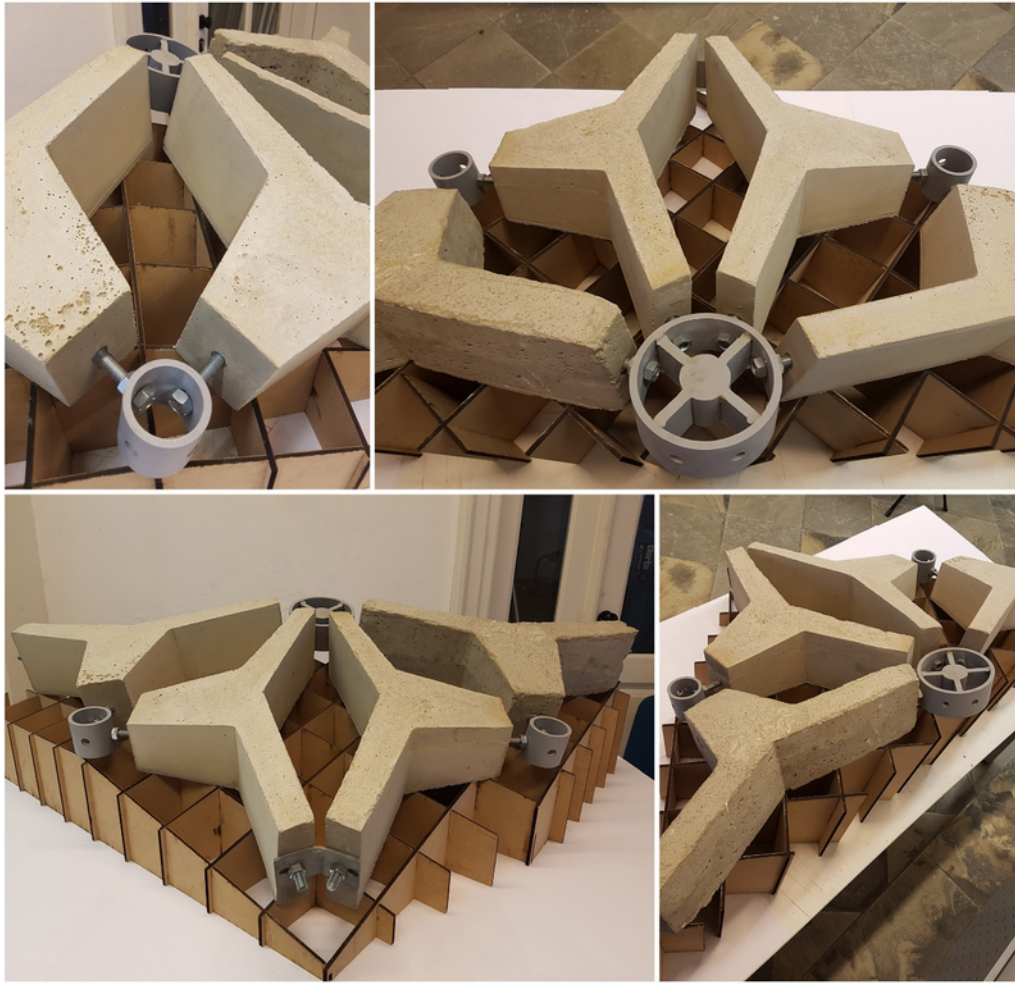


Fig. 32. Prototype of four structural elements adjusted using the two types of joints (Joint A and Joint B).

two times higher than the fabrication time of suggested formwork, given that in the former case 154 units of formwork must be fabricated while in the latter case only 15 units. At the level of concrete curing, 2 repetitions are required for the total completion of the overall shape in the case of conventional formwork having the half of units, which is approximately 2 working days of the overall construction. The respective repetitions needed with the proposed automated process are 21 having 15 adaptable formworks for the curing of concrete in parallel. In both methods, a time frame of 40 working days approximately is needed to complete the overall casting and curing.

Conclusions

The computational design optimization process introduced in this paper is examined on the basis of material waste minimization, aiming to offer a low environmental impact solution as well as on the basis of flexibility of reconfigurable formwork involved, aiming to produce variable modular element solutions for the development of complex shell-structures. This might open the possibility for suggesting formwork systems able to be fabricated in short time period and in lower cost, enabling at the same time large variety of their shape alternation to be achieved, without the necessity for developing large number of custom formworks, which could be one-off solutions, increasing at the same time material waste. Having said this, the increased working time required by the adaptive formwork during concrete curing cannot be ignored. This is because of the limited number of formwork used in

construction process but also due to the curing properties of the concrete material involved.

All the above, showed that the suggested procedure has advantages and disadvantages for implementation in actual construction cases. Nevertheless, this incident cannot ignore the possibilities that can open in the construction industry for free-form shell structures construction. At the same time, the suggested workflow is able to satisfy sustainable aspects, especially when is applied in the early design phase of shell structures that are further planned to be physically produced in actual scale. By combining computational design based on topology optimization concepts with innovative automated construction principles, and specifically by using reconfigurable formwork mechanisms, any custom geometrical configuration of structural modular members can be captured. Within this framework, the development of various shell structure morphologies can be optimized towards their structural efficiency and material minimization.

Further work will focus towards two directions. Firstly, towards the improvement of the suggested computational design optimization approach in terms of its interoperability, aiming to achieve a more direct communication and exchange of information between the various steps of the process at a digital level. In turn, this will allow effective integration among the results obtained during different phases of investigation, like form-finding, tessellation, topology optimization and material distribution.

Another future direction of investigation that is of high significance and can build on the existing proof-of-concept nature of the presented

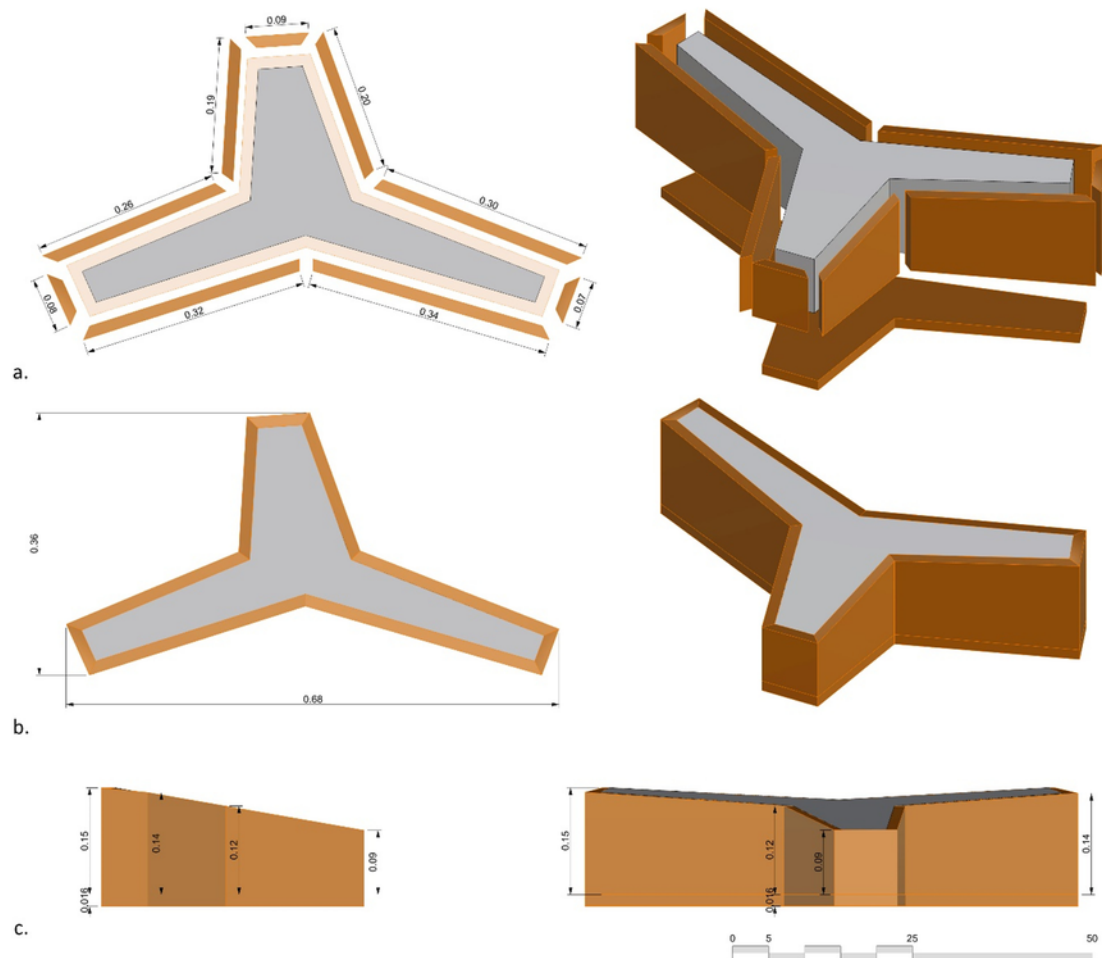


Fig. 33. The conventional formwork for a typical unit. a) The wooden parts b) The assembly c) Elevation.

Table 1
Time for formwork prototyping and for series production.

Formwork prototyping	Hours	
	Prototype development	Series production
Woodwork	7	1
Metalwork	16	4
Other works and fixing	12	3
Total	35	8

work, is the investigation of free-form shell structures based on a more comprehensive and accurate examination of their structural behavior. This will be achieved by including structural constraints and load combinations, in order to capture real case scenarios and accurate results of the structural load-bearing behavior. Also, investigation, selection and introduction of alternative materials including concrete mixtures will allow a more thorough understanding of the behavior of the material applied, information that can be incorporated during the computational analysis phase. Additionally, the improvement of the construction process as a whole, as well as of the reconfigurable mechanism, the structural members manufacturing and their assembly are directions that open possibilities for experimentation. In terms of the reconfigurable modular formwork, an attempt to replace parts of the mechanism could make the process of formwork preparation, casting and demolding less time consuming. For instance, more effective control of the movement of the three nodes need to be achieved, as well as more

robust control of the three midpoints defining the thickness of the structural modules are necessary within the formwork improvement. In addition, an attempt to investigate the possibility of introducing a fully automated system, which includes actuators for shape readjustment of the formwork will be examined.

Acknowledgments

This work was supported by the research program Optimization Driven Architectural Design of Structures (OptArch) that is funded by the European Commission under the framework of Marie Skłodowska-Curie Actions, Research and Innovation Staff Exchange (RISE), Call: H2020-MSCA-RISE-2015 [grant numbers 689983].

Table 2
Materials used for formwork prototype development and their cost.

Formwork materials and cost				
Components	Type	Quantity	Cost per unit (Euro)	Total cost (Euro)
Timber	{laser cut} MDF 6 mm	1		5.7
	120 × 120 cm Marine Plywood	3		6.82
	75 × 75 × 2 cm Wood	2		2
	69 × 6 × 3 cm {laser cut}	3		2
Fabric	Elastic Tarpaulin 90 × 15 cm			
Sliding system	Galvanized steel track	2		16–17
	30 × 33,5 mm. Thickness 1,5 mm (OMGE Art.20) 70 cm Adjustable steel roller with Ø 24 mm bearing steel wheels (OMGE Art.23)	2		
St. Compression Spring	MA05-8X1.0X1M 40 mm	1	per 1 m	3.4
Wood Screws	40 mm	4		0.2
Galv. Turnbuckle	eye-eye 5 mm	3	0.89	2.67
St. Axle	6 mm 15 cm	3	per 1 m - 0.49	0.98
	6 mm 20 cm	6		
Galv. Pipes	175 × 20 mm. Thickness 2 mm	6		10
Galv. Wing nuts	6 mm ZPL DIN315	3	0.08	0.24
Wing screw	4 × 25 mm ZPL D316	3	0.6	1.8
Disc Knob open	6 mm black	3	1.5	4.5
Teflon Rod	20 mm 2.5 cm	3	per 1 m - 5.59	5.59
Plastic Plug	22 mm external black	3	4pcs package	0.39
St. Hinge	Loose pin 75X50x2 mm	2	0.23	0.46
Sheet iron	100 × 60 × 2 mm	4		3
St. Angle Bracket	40 × 40 × 50 mm	3	0.5	1.5
	25 × 25 × 20 mm	2	0.25	0.5
St. Door Bolt	40 × 20 mm	3	2	6
Wood Screws	20 mm	~20		0.5
Glue	Fabric to metal	1		6
Paint	Spray Zinc Grey 400 ml	1		3.25
Releasing Oil	Multi-purpose lubricant 200 ml (not used)	1		7
Total cost (Euro)				88.10

Table 3
Material proportions of the suggested concrete mixture.

Concrete mixture	
Material	Proportion (containers)
Pearlite (Dioperli)	12
Cement (Portland)	4
Extra fast setting cement (Durofast)	3

Table 4
Various activities involved and average time needed during the construction of a custom structural element prototype.

Activities	Average time (hours)
Formwork cleaning	20/60 = 0.33
Formwork readjustment	45/60 = 0.75
Concrete mixture creation	10/60 = 0.16
Concrete mixture casting	10/60 = 0.16
Concrete curing	1350/60 = 22.5
Demolding	5/60 = 0.083
Total time (hours)	24

Table 5
Fabrication cost of conventional formwork.

	Quantity		Total cost (Euro)
Material cost (Euro/Unit)			
• Marine plywood (18 mm)	20	154	3080
Labor cost (Euro/Unit)			
• 1 skilled labor/2 h – 20 euros	20	154	3080
Overhead cost (Euro/Unit)			
• Extra complexity charge and auxiliary equipment (15%)	8	154	1232
Total conventional formwork fabrication cost (Euro)			7392

Table 6
Fabrication cost of reconfigurable formwork.

	Quantity		Total cost (Euro)
Material cost (Euro/Unit)			
• Reconfigurable formwork (Table 2)	88	15	1320
Labor cost (Euro/Unit)			
• 1 skilled labor (2 h-20euros)	35080	114	3501120
First unit prototype (35 h/unit)			
Series production (8 h/unit)			
Total reconfigurable formwork fabrication cost (Euro)			2790

Table 7
Fabrication time of conventional formwork.

	Quantity		Total time (hours)
Time for conventional formwork fabrication (hours/unit)			
• 1 skilled labor (2 h-20euros)	2	154	308
Total conventional formwork fabrication time (Hours)			308

Table 8

Fabrication time of reconfigurable formwork.

	Quantity	Total time (hours)
Time for reconfigurable formwork fabrication (hours/unit)		
• 1 skilled labor (2 h-20euros)	358	114
First unit prototype		35112
Series production		
Total reconfigurable formwork fabrication time (Hours)		147

Table 9

Comparison between total working days of formwork fabrication and curing of conventional and reconfigurable formwork.

Working days for formwork fabrication and curing (day/unit)	Quantity	Total working days (days)
Conventional formwork fabrication		
• Labor working days (2 h = 0.25 day per unit)	1542 repetitions (308 units)	38.51.8
• Curing time (22.5 h = 0.93 day per 154 units)		
Total working days for conventional formwork fabrication and curing time (days)		40.3
Reconfigurable formwork fabrication		
• Labor working days (9.8 h = 1.22 days per unit)	1521 repetitions (308 units)	18.319.7
• Curing time (22.5 h = 0.93 day per 15 units)		
Total working days for reconfigurable formwork fabrication and curing time (days)		38

References

- [1] F. Gramazio, K. Kohler, *Made by robots: challenging architecture at a larger scale*, Architecture Design, Wiley, 2014 (ISBN: 978-1-118-53548-6).
- [2] J. Willmann, M. Knauss, T. Bonwetsch, A.A. Apolinarska, F. Gramazio, M. Kohler, Robotic timber construction. Expanding additive fabrication to new dimensions, *Autom. Constr.* 61 (2016) 16–23, doi:10.1016/j.autcon.2015.09.011.
- [3] E. Lloret, A.R. Shahab, M. Linus, R.J. Flatt, F. Gramazio, M. Kohler, S. Langenberg, Complex concrete structures. Merging existing casting techniques with digital fabrication, *Comput. Aided Des.* 60 (2015) 40–49, doi:10.1016/j.cad.2014.02.011.
- [4] D. Asprone, C. Menna, F.P. Bos, T.A.M. Salet, J. Mata-Falcón, W. Kaufmann, Re-thinking reinforcement for digital fabrication with concrete, *Cem. Concr. Res.* 112 (2018) 111–121, doi:10.1016/j.cemconres.2018.05.020.
- [5] I. Agustí-Juan, G. Habert, Environmental design guidelines for digital fabrication, *J. Clean. Prod.* 142 (2017) 2780–2791, doi:10.1016/j.jclepro.2016.10.190.
- [6] B. García de Soto, I. Agustí-Juan, J. Hunhevicz, S. Joss, K. Graser, G. Habert, B.T. Adey, Productivity of digital fabrication in construction: cost and time analysis of a robotically built wall, *Autom. Constr.* 92 (2018) 297–311, doi:10.1016/j.autcon.2018.04.004.
- [7] I. Paoletti, Mass customization with additive manufacturing: new perspectives for multi performative building components in architecture, *Proc. Eng.* 180 (2017) 1150–1159, doi:10.1016/j.proeng.2017.04.275.
- [8] D. Delgado Camacho, P. Clayton, W.J. O'Brien, C.C. Seepersad, M. Juenger, R. Ferron, S. Salamone, Applications of additive manufacturing in the construction industry – a forward-looking review, *Autom. Constr.* 89 (2018) 110–119, doi:10.1016/j.autcon.2017.12.031.
- [9] S.O. Ajayi, L.O. Oyedele, O.O. Akinade, M. Bilal, H.A. Alaka, H.A. Owolabi, K.O. Kadiri, Attributes of design for construction waste minimization: a case study of waste-to-energy project, *Renew. Sust. Energ. Rev.* 73 (2017) 1333–1341, doi:10.1016/j.rser.2017.01.084.
- [10] S.H. Ghaffar, J. Corker, M. Fan, Additive manufacturing technology and its implementation in construction as an eco-innovative solution, *Autom. Constr.* 93 (2018) 1–11, doi:10.1016/j.autcon.2018.05.005.
- [11] G. Kazakis, I. Kanellopoulos, S. Sotiropoulos, N.D. Lagaros, Topology optimization aided structural design: interpretation, computational aspects and 3D printing, *Heliyon* 3 (10) (2017), doi:10.1016/j.heliyon.2017.e00431 e00431.
- [12] J.F.V. Vincent, Biomimetic materials. Material experience, *Fundamentals of Materials and Design*, 2002, pp. 235–246.
- [13] J.F.V. Vincent, Survival of the cheapest, *Mater. Today* 5 (12) (2002) 28–41, doi:10.1016/S1369-7021(02)01237-3.
- [14] M. Pawlyn, *Biomimicry in Architecture*, 1st edition, RIBA Publishing, 2011 (ISBN: 978-1859463758).
- [15] R. Finsterwalder, *Form Follows Nature*, Springer, 2011.
- [16] W.D. Thompson, *On Growth and Form*, Cambridge University Press, Cambridge, 1992 (ISBN: 978-0521437769).
- [17] J. Knippers, K.G. Nickel, T. Speak, *Biomimetic research for architecture and building construction*, Biological Design and Integrative Structures, Springer, 2016.
- [18] G. Pohl, W. Natchigall, *Biomimetics for Architecture & Design*, Springer, 2015.
- [19] A. Hosny, N. Jacobson, z Seibold, *Voxel Beam, Emerging Experience in Past, Present and Future of Digital Architecture*, Proceedings of the 20th International Conference of the Association for Computer-Aided Architectural Design Research in Asia CAADRIA 2015, Daegu 20–22 May 2015, 2015, pp. 755–764.
- [20] S. Białkowski, A. Kepczynska-Walczak, Engineering tools applied in architecture. - challenges of topology optimization implementation, *Real Time - Proceedings of the 33rd eCAADe Conference - Volume 1*, Vienna University of Technology, Vienna, Austria, 16–18 September 2015, 2015, pp. 261–268 (ISBN: 97894912070082).
- [21] J. Burry, P. Felicetti, J. Tang, M. Burry, M. Xie, Dynamical structural modelling. A collaborative design exploration, *Architecture in the Network Society*, 22nd eCAADe Conference Proceedings, Copenhagen, Denmark, 15–18 September 2004, 2004, pp. 312–317 (ISBN: 0-9541183-2-4).
- [22] S. Białkowski, Structural optimisation methods as a new toolset for architects, in: A. Hernejoja, T. Österlund, P. Markkanen (Eds.), *Complexity & Simplicity - Proceedings of the 34th eCAADe Conference - Volume 2*, University of Oulu, Oulu, Finland, 22–26 August 2016, 2016, pp. 255–264.
- [23] Why design for AM must progress [online] Available at: <https://www.develop3d.com/comment/the-university-of-nottingham-professor-christopher-tuck-manufacturing> 29 June 2018
- [24] N. Gardan, A. Schneider, Topological optimization of internal patterns and support in additive manufacturing, *J. Manuf. Syst.* 37 (2015) 417–425, doi:10.1016/j.jmsy.2014.07.003.
- [25] M. Donofrio, Topology optimization and advanced manufacturing as a means for the design of sustainable building components, *Proc. Eng.* 145 (2016) 638–645, doi:10.1016/j.proeng.2016.04.054.
- [26] Weight watchers [online] Available at: <https://www.develop3d.com/profiles/weight-watchers-Light-Rider-3D-printing-topology-optimisation-design> 29 June 2018
- [27] S. Galjaard, S. Hofman, N. Perry, S. Ren, Optimizing structural building elements in metal by using additive manufacturing, *Proceedings of the Annual International Association for Shell and Spatial Structures (IASS 2015)*, Amsterdam, Netherlands, 2015, pp. 17–20 August 2015.
- [28] H. Ohmori, Computational morphogenesis: its current state and possibility for the future, *Int. J. Space Struct.* 25 (2) (2010) 75–82, doi:10.1260/0266-3511.25.2.75.
- [29] C. Cui, H. Ohmori, M. Sasaki, Computational morphogenesis of 3D structures by extended ESO method, *J. Int. Assoc. Shell Spat. Struct.* 44 (1) (2003) 51–61.
- [30] T. Sakamoto, *From control to design*, Actar, 2009.

- [31] Sawapan [online] Available at: <http://www.sawapan.eu/25 May 2017>
- [32] Millipede [online]. Available at: http://www.sawapan.eu/sections/section88_Millipede/files/MillipedeMarch2014.pdf 25 May 2017
- [33] Ameba [online] Available at: https://ameba.xieym.com/index_en/30 December 2018
- [34] Grasshopper [online] Available at: <http://www.grasshopper3d.com/25 May 2017>
- [35] Rhino 3D [online] Available at: <https://www.rhino3d.com/25 May 2017>
- [36] P. Dombrowsky, A. Søndergaard, Three-dimensional topology optimisation in architectural and structural design of concrete structures, in: D. Alberto, L. Carlos (Eds.), *Evolution and Trends in Design: Analysis and Construction of Shell and Spatial Structures*, CMD Domingo y Lázaro Ingenieros SL, 2009, pp. 268–269.
- [37] J. Feringa, A. Søndergaard, Design and fabrication of topologically optimized structures; an integral approach a close coupling form generation and fabrication, in: H. Achten, J. Pavlicek, J. Hulín, D. Matejovská (Eds.), *Digital Physicality – Proceedings of the 30th International Conference on Education and Research in Computer Aided Architectural Design in Europe*, Prague, Czech Republic, September 12–14, 2012, Volume 1, eCAADe (Education and research in Computer Aided Architectural Design in Europe) and ČVUT, Faculty of Architecture, Prague, Czech Republic, 2012, pp. 487–490.
- [38] D. Veenendaal, P. Block, Design process for prototype concrete shells using a hybrid cable-net and fabric formwork, *Eng. Struct.* 75 (2014) 39–50, doi:10.1016/j.engstruct.2014.05.036.
- [39] M. Shaffer, Developing robotic formwork: enhancing formwork mobility and variability through mechanization, *Construction Robot.* 1 (2017) 77–83, doi:10.1007/s41693-017-0004-4.
- [40] H.R. Schipper, S. Grünwald, Efficient material use through smart flexible formwork method, *ECO-Crete: International Symposium on Environmentally Friendly Concrete*, Reykjavik, Iceland, 13–15 August 2014, 2014. <http://resolver.tudelft.nl/uuid:5f767d7f-6ad1-4e37-9efc-1817e9561274>. [accessed 31 December 2018].
- [41] B. Koc, S. Thangaswamy, Design and analysis of a reconfigurable discrete pin tooling system for molding of three-dimensional free-form objects, *Robotics and Computer-Integrated Manufacturing*, 27 (2), Pergamon Press, 2011, pp. 335–348, doi:10.1016/j.rcim.2010.07.017.
- [42] Khabazi, Z., Budig, M., 2016. Adaptive Fabrication Cellular Concrete Casting Using Digital Moulds. Herneoja, Aulikki; Toni Österlund and Piia Markkanen (eds.), *Complexity & Simplicity - Proceedings of the 34th eCAADe Conference - Volume 1*, University of Oulu, Oulu, Finland, 22–26 August 2016, pp. 83–92, (ISBN: 978-9491207105).
- [43] Mars Pavilion [online]. Available at: <http://www.formfounddesign.com/palm-springs-pavilion> 25 May 2017
- [44] Robotic casting [online] Available at: <http://www.robarch2012.org/677/new-workshop-announced-harvard-robarch-201229 June 2018> Robotic Casting [online]. Available at: <http://www.robarch2012.org/677/new-workshop-announced-harvard-robarch-2012> [Accessed 29 June 2018].
- [45] Warszawski, A., 1984. Economic evaluation of robotics in building, *Proceedings of the 1st International Symposium on Automation and Robotics in Construction (ISARC)*, Pittsburgh, USA, pp. 41–58, <http://dx.doi.org/10.22260/ISARC1984/0004>.
- [46] M.J. Skibniewski, Framework for decision-making on implementing robotics in construction, *J. Comput. Civ. Eng.* 2 (2) (1988) 188–201, doi:10.1061/(ASCE)0887-3801(1988)2:2(188).
- [47] B.G. De Soto, I. Agustí-Juan, J. Hunhevicz, S. Joss, K. Graser, G. Habert, B.T. Adey, Productivity of digital fabrication in construction: cost and time analysis of a robotically built wall, *Autom. Constr.* 92 (2018) 297–311, doi:10.1016/j.autcon.2018.04.004.
- [48] A.S. Hanna, *Concrete Formwork Systems*, Taylor and Francis, New York, 1998.
- [49] S. Hickert, U. Knaack, Evaluation of free-form concrete architecture, moulding systems and their technical potentials, *J. Facade Des. Eng.* 3 (3–4) (2015) 273–288, doi:10.3233/FDE-160045.
- [50] G. Tang, An overview of historical and contemporary concrete shells, their construction and factors in their general disappearance, *Int. J. Space Struct.* 30 (1) (2015) 1–12. <https://journals.sagepub.com/doi/10.1260/0266-3511.30.1.1>.
- [51] K. Nassar, E.A. Aly, Automated planning and design of formwork for freeform shell structures, *Construction Research Congress 2012*, West Lafayette, Indiana, United States, 21–23 May 2012, 2012, pp. 1165–1174, doi:10.1061/9780784412329.117.
- [52] C. Gomes, M. Parente, M. Azenha, J.C. Lino, An integrated framework for multi-criteria optimization of thin concrete shells at early design stages, *Adv. Eng. Inform.* 38 (2018) 330–342, doi:10.1016/j.aei.2018.08.003.
- [53] W.J. Hawkins, M. Herrmann, T.J. Ibell, B. Kromoser, A. Michaelski, J.J. Orr, R. Pedreschi, A. Pronk, H.R. Schipper, P. Shepherd, D. Veenendaal, R. Wansdronek, M. West, Flexible formwork technologies - a state of the art review, *Struct. Concr.* 17 (6) (2016) 911–935, doi:10.1002/suco.201600117.
- [54] Kangaroo physics [online] Available at: <http://www.food4rhino.com/app/kangaroo-physics> 25 May 2017 Kangaroo Physics [online]. Available at: <http://www.food4rhino.com/app/kangaroo-physics> [Accessed 25 May 2017].
- [55] Structural software for analysis and design | SAP2000 [online] Available at: <https://www.csiamerica.com/products/sap2000> 25 May 2017 Structural Software for Analysis and Design | SAP2000 [online]. Available at: <https://www.csiamerica.com/products/sap2000> [Accessed 25 May 2017].
- [56] H. Seifi, Y. Xie, J. O'Donnell, N. Williams, Design and fabrication of structural connections using bi-directional evolutionary structural optimization and additive manufacturing, *Appl. Mech. Mater.* 846 (2016) 571–576, doi:10.4028/www.scientific.net/AMM.846.571.
- [57] Q. Han, Y. Liu, Y. Xu, Study on the assembled hub joints in single-layer reticulated domes, in: A. Bögle, M. Grohmann (Eds.), *Proceedings of the IASS Annual Symposium 2017 “Interfaces: Architecture. Engineering.science”*, Hamburg, Germany, 2017.
- [58] H. Seifia, A.R. Javana, S. Xua, Y. Zhaob, Y.M. Xie, Design optimization and additive manufacturing of nodes in gridshell structures, *Eng. Struct.* 160 (2018) 161–170, doi:10.1016/j.engstruct.2018.01.036.
- [59] LunchBox [online] Available at: <http://www.food4rhino.com/app/lunchbox> 25 May 2017
- [60] Anon [online]. Available at: http://www.halfen.com/application/filebrowser/library/de/media/catalogues/DEMU_FIX_14-E.pdf [Accessed 25 May 2017].
- [61] M. Mihailescu, R. Sundaram, Construction methods and quality control for concrete shell roofs, in: A. Domingo, C. Lazaro (Eds.), *Evolution and Trends in Design, Analysis and Construction of Shell and Spatial Structures - Proceedings of the International Association of Shell and Spatial Structures (IASS) Symposium 2009*, Universidad Politecnica de Valencia, Valencia, Spain, 2009, pp. 177–197 28 September – 2 October 2009. (ISBN: 978-84-8363-459-2).
- [62] D. Wendland, Experimental construction of a free-form shell structure in masonry, *Int. J. Space Struct.* 24 (1) (2009) 1–11, doi:10.1260/026635109788251412.
- [63] M. Deuss, D. Panozzo, E. Whiting, Y. Liu, P. Block, O. Sorkine-Hornung, M. Pauly, Assembling self-supporting structures, *ACM Trans. Graph.* 33 (6) (2014) 1–10. <http://doi.acm.org/10.1145/2661229.2661266>.